EXPERIMENTAL STUDY OF EFFECTS OF SIMULATED NEUTRALIZED SOLAR WIND ON WHITE-PIGMENT THERMAL CONTROL COATINGS

By Lawrence B. Fogdall, Sheridan S. Cannaday,
Fredrick D. Reinke and Barbara K. Madaras

October 1969

Prepared under Contract No. NAS2-5343 by

THE BOEING COMPANY
Aerospace Group

Seattle, Washington

for

AMES RESEARCH CENTER
NATIONAL AERONAUTICS AND SPACE ADMINISTRATION

NASA CR

EXPERIMENTAL STUDY OF EFFECTS OF SIMULATED NEUTRALIZED SOLAR WIND ON WHITE-PIGMENT THERMAL CONTROL COATINGS

By Lawrence B. Fogdall, Sheridan S. Cannaday,
Fredrick D. Reinke and Barbara K. Madaras

October 1969

Prepared under Contract No. NAS2-5343 by

THE BOEING COMPANY
Aerospace Group

Seattle, Washington

for

AMES RESEARCH CENTER
NATIONAL AERONAUTICS AND SPACE ADMINISTRATION

ABSTRACT

An experimental program to obtain information about the neutralization properties of the simulated solar wind has been conducted. Selected thermal control coatings were exposed to the simulated solar wind and solar electromagnetic radiation environment. Duplicate exposures except for the presence or absence of "thermal" electrons to neutralize the 1-keV proton component of the space radiation environment were performed. Effects of each component of the simulated environment, and effects of the entire combined environment, as manifested in changes in reflectance properties of the coating specimens, were ascertained. Reflectance degradation resulting from exposure to the overall combined environment generally was found to be less than the sum of degradations sustained by exposure to components of the space environment. In contrast to predictions, the presence of "thermal" electrons as an additional component in half of the simulated environmental exposures resulted in only somewhat heavier damage to the reflectance properties of the coatings. Thus, the long-observed discrepancy between heavy coating damage indicated by interplanetary space flight data, and less damage shown by laboratory simulation of the interplanetary space environment is reduced, but still remains. Plausible reasons for the continuing discrepancy and logical future efforts to resolve it are outlined.

KEY WORDS AND SYMBOLS

Electron
Emittance (ϵ)
Kilo electron volt (keV)
Proton
Reflectance
Solar absorptance (α_s)
Solar wind
Thermal control coating
Ultraviolet radiation
Vacuum

ACKNOWLEDGMENTS

The results, conclusions, and recommendati . being reported herein were obtained in an experimental program conducted by The Boeing Company at Seattle, Washington between March and August 1969. The government's technical monitor for the Contract (NAS2-5343) was Mr. Elmer Streed, Chief, Vehicle Systems Design Branch, Ames Research Center of the National Aeronautics and Space Administration. Within Boeing, Mr. Richard R. Brown was program leader, Mr. Lawrence B. Fogdall was technical leader, and Mr. Sheridan S. Cannaday was principal investigator. The technical contributions of Mrs. Barbara K. Madaras and Messrs. Fredrick D. Reinke and Loren D. Milliman are gratefully acknowledged.

CONTENTS

ILLUSTRATIONS

ILLUSTRATIONS (Continued)

TABLES

INTRODUCTION

The Solar Wind Environment

Present understanding of the solar wind indicates that it consists of a macroscopically neutral flux of electrons, protons, alpha particles, and heavier ions, flowing radially from the sun. The average proton density is approximately 5 cm^{-3}, with an average velocity of 500 km/sec. Thus, the proton flux is approximately 2.5×10^8 cm^{-2} sec^{-1}, with the protons having an average energy of about 1 keV (kiloelectron volts). Alpha particles, as well as heavier ions, have average velocities similar to that of the protons. The alpha to proton number density ratio varies between 0.5 percent and 15 percent, whereas heavier ions exist in much smaller numbers. These data have been obtained and confirmed during various space probe missions, including the Mariner Venus and Mars probes and the Pioneer 6 space probe (References 1 through 3).

The density and energy spectrum of the solar wind electron component is less well determined. Assuming that all particles are emitted with equal radial velocities, the electron energy can be determined from its mass ratio to the proton, giving an electron energy of approximately 1 eV. However, measurements of the electron temperature indicate that it is 2 to 5 times the proton-ion temperature, with a typical value of 2×10^5 °K (Reference 4). In Reference 5, Frank obtains a value of 0.05 cm^{-3} for the number density of electrons greater than 33 eV, with a temperature of 8×10^5 °K and a plasma bulk velocity of 400 km/sec. The thermal energy of the electrons ranges, then, from 15 to 70 eV, while the thermal energies of the 1-keV protons are less than 15 eV. This means that the flux levels of the electrons can be greater than the proton flux levels within the neutral plasma. Since these data for the electron distribution must be considered preliminary, complete simulation of the solar wind electron component awaits clarification of the actual environment.

Program Description

In the above context, the experiments performed in this study represent a preliminary simulation of the solar space environment. The objective has been to compare the effects of the "neutralized" solar wind with the effects of its proton component alone, with the comparison to be performed both in the presence and in the absence of simulated solar ultraviolet radiation.

Concern for proper simulation techniques has been of major interest during the program, arising from the assumption that the thermal electrons present in the solar wind may contribute significantly to space radiation effects on thermal control coatings. Moreover, numerous and well-documented observations of synergistic effects (as in References 6 and 7) imply that tests for performance in a multi-radiation source environment are inconclusive without actual tests in a reasonable simulation of that environment. Thus the radiation exposures for this program have been conducted in accordance with the following parameters:

- monoenergetic protons of 1-keV energy, to be representative of the range of energies of solar wind protons;
- monoenergetic electrons of 25-eV energy, to be representative of the energy spread of solar wind "thermal" electrons;
- particle exposure rates of 1×10^{10} cm^{-2} sec^{-1}, which is more than ten-fold acceleration over space values;
- continuum ultraviolet radiation between wavelengths of 0.2 and 0.4 microns, at approximately a 3-space-sun rate; and visible and near infrared radiation at approximately a 2-space-sun rate;
- chamber vacuum of 5×10^{-7} torr or better;
- temperature control of the substrates of coating specimens at 291 ± 2 °K (18 ± 2 °C);
- magnetic analysis of the proton source output to separate H^+ ions from other species.

It is realized that improvements in the degree of simulation are still possible, particularly in the areas of radiation type (alpha particles and multi-energy protons instead of monoenergetic protons) and equal exposure ratios, or the same laboratory acceleration factor for both particles and solar electromagnetic radiation.

EXPERIMENTAL PROGRAM

Facility Description

The experimental work has been conducted using the Boeing combined radiation effects test chamber (CRETC) and low energy particle accelerator (LEPA). Overall descriptions of the equipment and its capabilities are contained in Reference 8; those features of particular interest for this program are further detailed here.

The accelerator employs an Ortec 501 RF ion source, which is capable of supplying either hydrogen or helium ions with several species. Magnetic deflection is used to analyze the ion output and separate the chosen component or specie (in this case protons) for injection into the CRETC (Figure 1).

Several modifications within the CRETC have made the results of this program possible. An Einzel lens (in addition to a similar one employed at the LEPA ion source) along the positive beam axis provides a measure of magnetic defocusing for enlarging the proton beam size. Between this lens and the coating sample array being exposed there is placed a very low energy ("thermal") electron source consisting of two low-work-function thermionic filaments that can be biased relative to the sample holders, which are at chamber ground potential (Figure 2). Each filament employs a platinum mesh strip which is dipped into a mixture of barium carbonate and strontium carbonate. The carbonates are converted in vacuum into barium oxide and strontium oxide. This filament configuration, having a high ratio of sample distance to proton beam diameter, results in reasonably efficient and uniform neutralization characteristics for the positive ion (proton) beam. A bias of 25 volts provides a reasonable acceleration of electrons to the sample plane at ground.

Several steps taken result in minimizing any potential charge buildup problems within the chamber which might affect either particle beam. It is possible to cover all dielectric materials other than coating samples with aluminum foil and provide good paths from foils to chamber ground (Figure 2). Whereas the CRETC normally employs a combination of cryogenic, ion, and turbomolecular vacuum

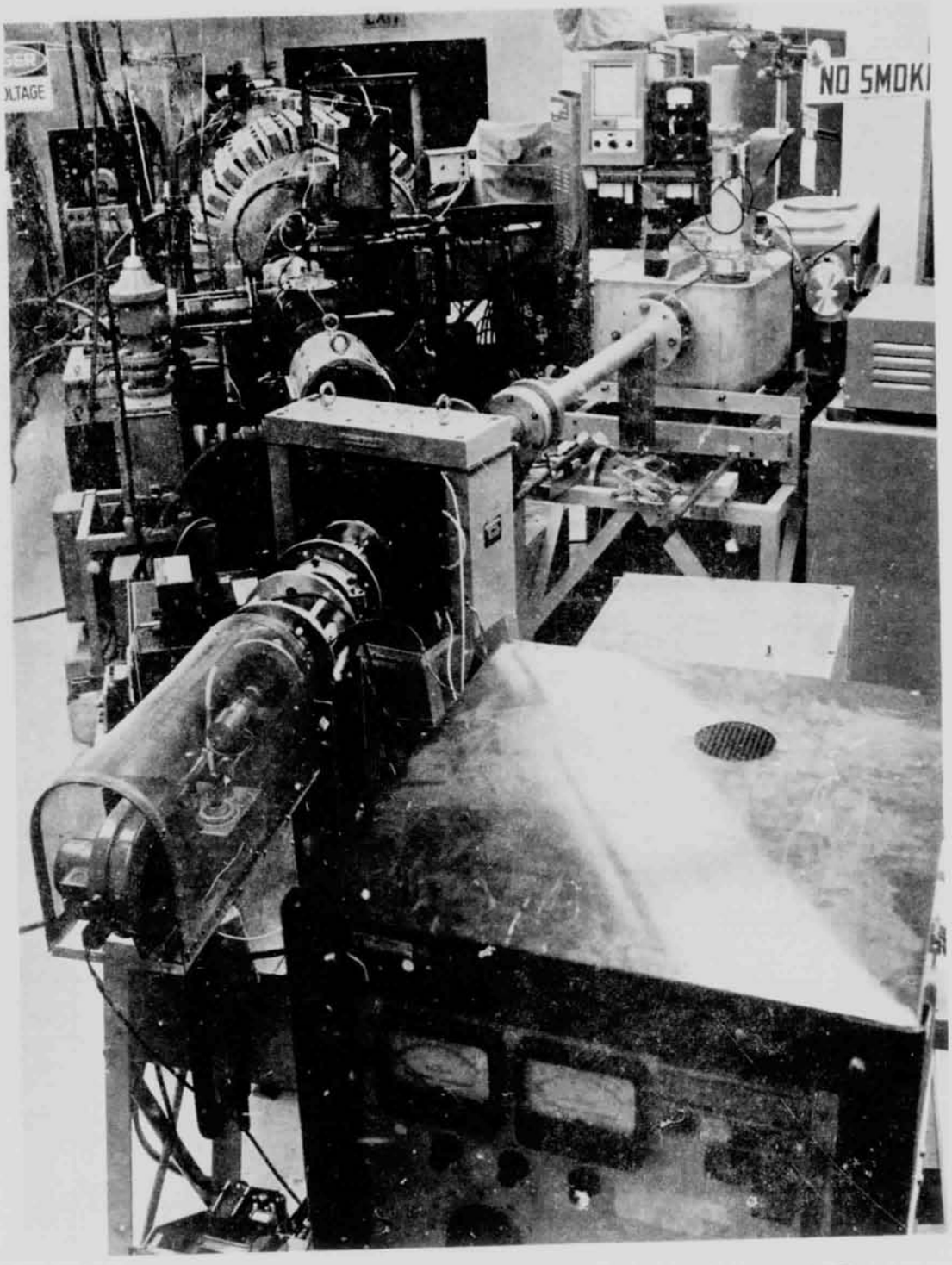

FIGURE 1. COMBINED RADIATION EFFECTS TEST CHAMBER AND LOW ENERGY PARTICLE ACCELERATOR

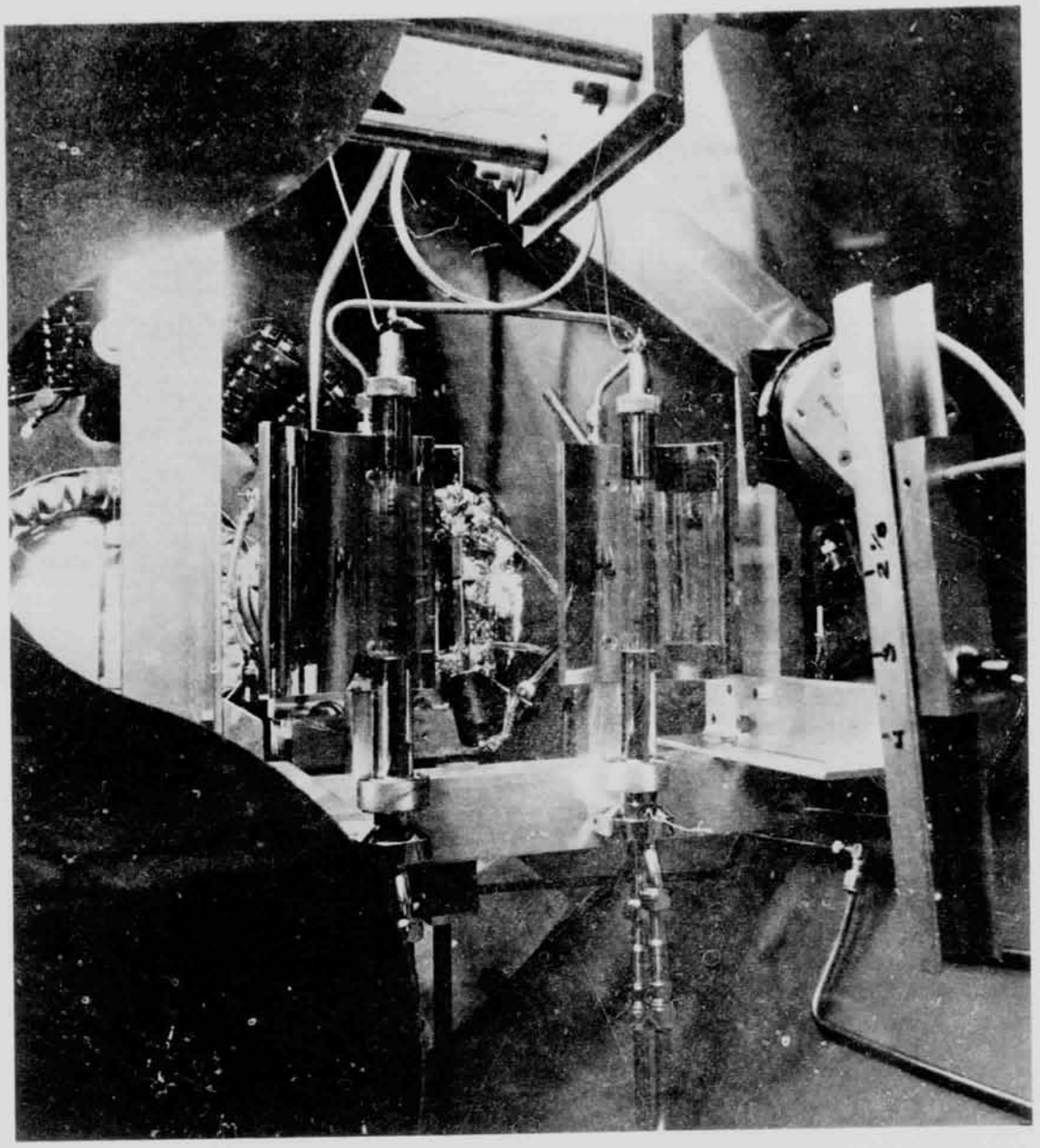

FIGURE 2. ULTRAVIOLET SOURCES, THERMAL ELECTRON ARRAY STRUCTURE, FARADAY CUP, AND RADIOMETER INSIDE CRETC

pumping, elimination of ion pump voltages (as high as 5 kV) within the chamber eliminates the possibility of stray fields competing with the 1-kilovolt proton potential and 25-volt electron potential difference. Removal of ion pump magnets from the chamber exterior eliminates stray magnetic fields.

The matrix or combination of environmental exposure conditions for this program has required rather elaborate measuring or "dosimetry" techniques. For measurement of ultraviolet radiation intensity a temperature-compensated TRW DR-2 radiometer (seen in Figure 2) maps the entire planar area which is occupied by coating samples during exposure. Filters allow a determination of the percentage of energy in the ultraviolet, and the resulting space ultraviolet sun rate. In addition to radiometer measurements before and after exposure, an in situ spectral monitoring of the xenon continuum (described in detail in Reference 8) provides an intermittent analysis of photon radiation level. The fact that the current through the water-cooled long-arc xenon sources (Figure 2) can be increased or decreased somewhat without exceeding their temperature limits or extinguishing their arcs provides a measure of compensation if lamp degradation occurs. Detection of lamp degradation and its spectral character is a principal assignment for the in situ monitor.

Particle dosimetry is performed by Faraday cups and copper discs. As described in Reference 8, two cups are movable, in horizontal and vertical arc-swinging fashion, to provide information about particle beam intensity as a function of angle from beam axis. A third, fixed Faraday cup behind the sample plane determines particle intensity or flux at the plane by virtue of its limiting apertures (one for each possible sample array) being in the sample wheel (Figure 3). Circular copper discs of the same size as test specimens are configured in a "dosimetry array" at positions equivalent to those occupied by coating specimens when exposed (Figure 3). The discs are insulated from the sample wheel (chamber ground), and via feedthroughs allow monitoring of particle beam profile prior to exposure and periodically during each exposure (when rotated into proper position). It is recognized that because of backscatter and secondary emission, such discs provide flux information relative to each other (uniformity of exposure at various sample positions), while the fixed Faraday cup most accurately determines absolute particle

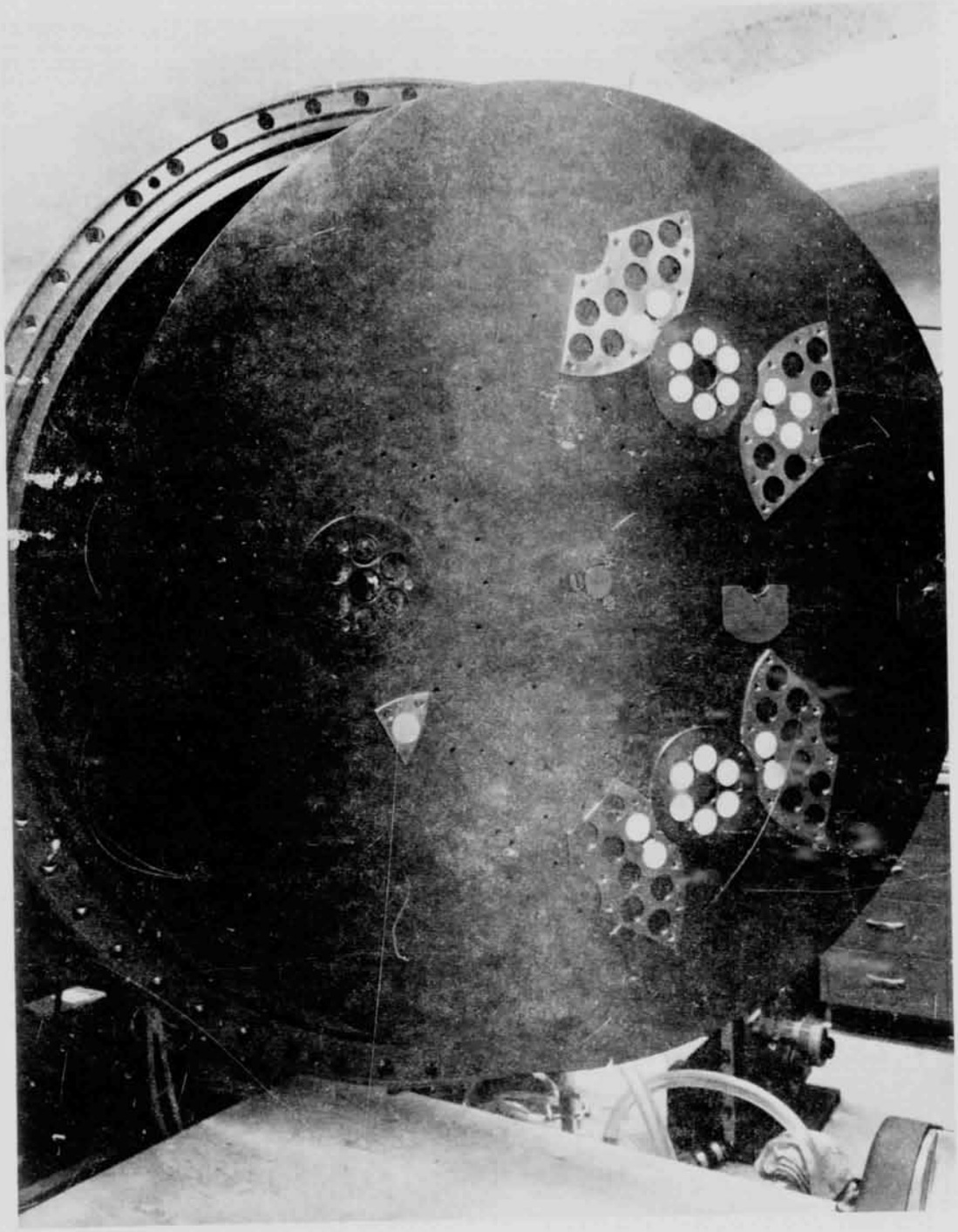

FIGURE 3. CRETC SAMPLE WHEEL, SAMPLE AND DOSIMETRY ARRAYS, AND FARADAY CUP APERTURES

flux. During dosimetry for and periodically during neutral beam exposures, proton-only flux levels and proton/thermal electron neutrality are determined by the same sensors, since the thermal electron filaments can be cooled momentarily.

One significant result of the program, based on the dosimetry portion alone, is that "entrainment" of thermal (10-100 eV) electrons in the 1-keV proton beam does not occur. That is, thermal electrons injected into the proton beam path are not constrained or confined to whatever region the proton beam occupies at a given time. Magnetic analysis of the positive beam provides a means for verifying this, by sweeping protons across a portion of the sample wheel. When this is done across dosimetry discs and Faraday cups with thermal electrons also present, deflection of the positive beam away from the discs and cups does not yield a zero or near-zero current reading. Such a reading would be indicative of entrainment of the electrons in the proton beam. Rather, indicated currents become negative to about the same extent as dosimetry-disc currents are positive in the case of protons alone. This implies a spatial distribution of thermal electrons which is largely independent of the presence of the proton beam. Further evidence is indicated by the requirement for symmetrical injection of thermal electrons into the proton beam even though injection occurs at a considerable distance from the sample plane. Injection by thermal electron sources which are not symmetrical about the beam axis results in asymmetrical neutralization.

Test Materials and Conditions

Two currently used types of spacecraft white thermal control coatings were selected for study in this program. The chief selection criterion was expected performance in a simulated space environment that could lead to a buildup of electrical charge in test specimens. Recognizing that single crystal zinc oxide is semiconducting, while aluminum oxide is insulating, led to the selection of zinc oxide pigment in potassium silicate (employed as an inorganic binder), and aluminum oxide pigment in the same binder material, for their predicted contrasting characteristics under proton exposure. It should be noted that the reflectance of the zinc oxide

coating (commonly known as Z-93) is generally found to be stable when exposed to ultraviolet and degradable under charged particle exposure, while coatings using wider band gap pigments such as aluminum oxide generally degrade in reflectance when exposed to ultraviolet radiation, but offer relative stability when exposed to protons alone. The results of this program are consistent with this general observation.

Test specimens of the selected thermal control coatings were prepared and furnished by the program sponsor, NASA-Ames Research Center, in the form of 15/16 ths-inch diameter coupons on aluminum substrates. Specifications of and preparation details for the test samples are given in Table 1.

Table 1. Coating Test Specimen Description and Preparation

Ames Coating N-1-45: Z-93-type zinc oxide in potassium silicate Ames Coating N-2-26 and -27: aluminum oxide in potassium silicate		
Material	Source	Comments
ZnO	New Jersey Zinc Co., SP-500, 99.9% pure; 0.25-0.35μ particle	P. B. R. - 5.2 Ball Milled with K_2SiO_3 4 hrs., sprayed 6 coats, overnight dry at 20°C, oven cured 1 hr at 150°C; 6 mils thick
Al_2O_3 (α)	Linde Division Union Carbide Co. 99.98% pure, 1.0μ particle	P. B. R. - 2.0 Ball Milled with K_2SiO_3 2 hrs., (same cure as above); 5.0 mils thick
K_2SiO_3	Sylvania Electronic Products PS-7 (35% solids)	

Multiple numbers of samples of each coating type have been exposed to the following array of simulated radiation environmental conditions:

- proton-only
- simultaneous proton/thermal electron (p/e)

- ultraviolet, visible, and near-infrared (for brevity, referred to hereinafter as ultraviolet)
- simultaneous ultraviolet/thermal electron (e/uv)
- simultaneous proton/ultraviolet (p/uv)
- simultaneous proton/thermal electron/ultraviolet (p/e/uv)

Data Collection and Processing

The reflectance of each coating test specimen and control specimen is measured before and after radiation exposure. Measurements are completed within about six hours after cessation of exposure. The reflectance measurement system includes an integrating sphere in vacuum, a far UV Beckman DK-2A spectrophotometer, a Datex SDS-1 automatic data collection system, and an IBM 526 card punch (see Reference 8).

Typical reproducibility of the reflectance measuring system is indicated by the stability of reflectance of a control specimen. Repeated measurements made on the control specimen before exposure and after each exposure segment result in nearly exact overlays of computer-processed output curves (Figure 4).

For accurate determination of reflectance properties and coating solar absorptance (α_s) values, the following procedure has been established. Each specimen reflectance measurement is made relative to the reflectance of the magnesium oxide coating on the integrating sphere wall. A comparison of this "normalized" reflectance characteristic is made with that obtained using an integrating sphere with sample-at-the-center technique, which is more widely regarded as delivering absolute reflectance data with higher accuracy, if imperfections in sphere wall uniformity and diffusivity are ignored. This establishes a "correction function" of reflectance versus wavelength. Separate, slightly different functions have been determined for diffuse and specular specimens. Results, as evidenced by the reflectance vs. wavelength plots and α_s values in this report, are in very good agreement with accepted values.

FIGURE 4. STABLE REFLECTANCE CHARACTERISTICS OF TEMPERATURE CONTROLLED Al_2O_3 - K_2SiO_3 WHITE COATING EXPOSED TO VACUUM

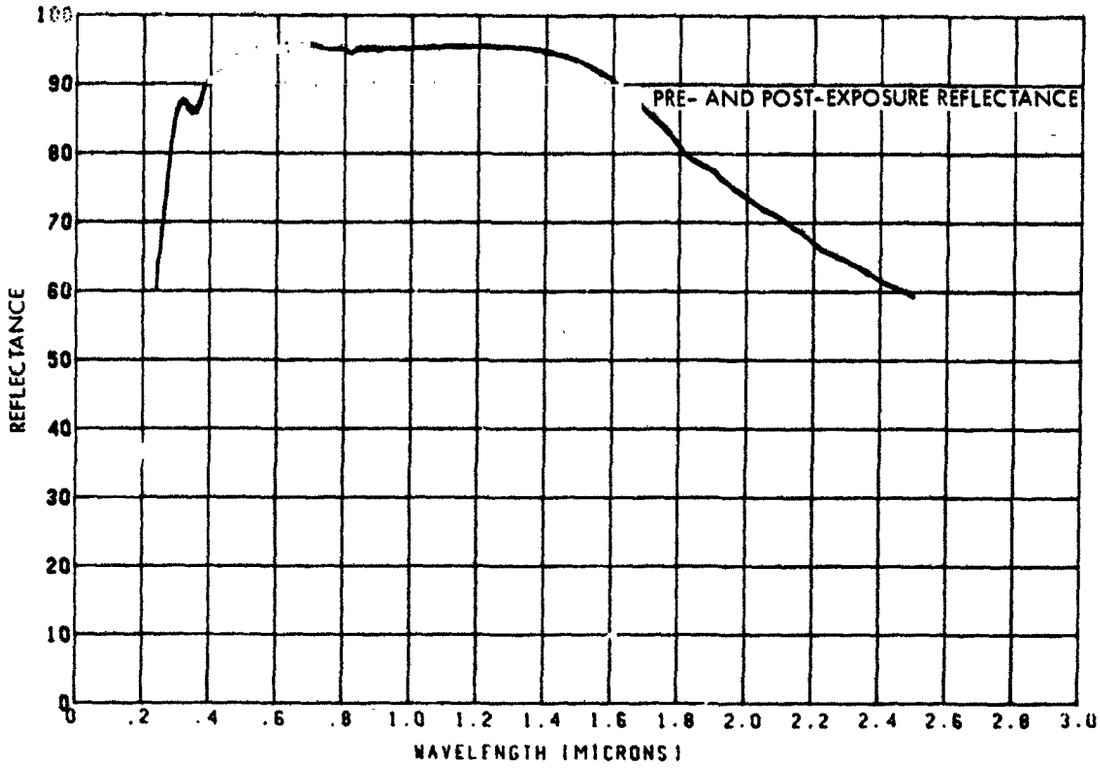

Experimental Results

Figures 5 through 10 present reflectance as a function of wavelength for Z-93 ($ZnO—K_2SiO_3$) exposed to six different environmental conditions. When exposed to 1-keV protons alone, Z-93 degrades in both the visible and the infrared regions (Figure 5). There is evidence of reflectance degradation beginning to saturate, especially in the infrared, as damage after 5×10^{15} protons/cm^2 is not much greater than the amount of degradation measured after exposure to 2×10^{15} protons/cm^2. Neutralization of the proton beam with 25-eV electrons results in saturation of the infrared-region damage at lower exposure fluences; Figure 6 shows that infrared reflectance values after 2×10^{15} protons/cm^2 and electrons/cm^2 are nearly identical to the values after 5×10^{15}. In the visible region, however, reflectance continues to degrade significantly as particle fluences increase beyond 2×10^{15}.

FIGURE 5. IN SITU EFFECTS OF 1-KEV PROTONS ON NASA-AMES Z-93 SP-500 ZINC OXIDE PIGMENT IN POTASSIUM SILICATE

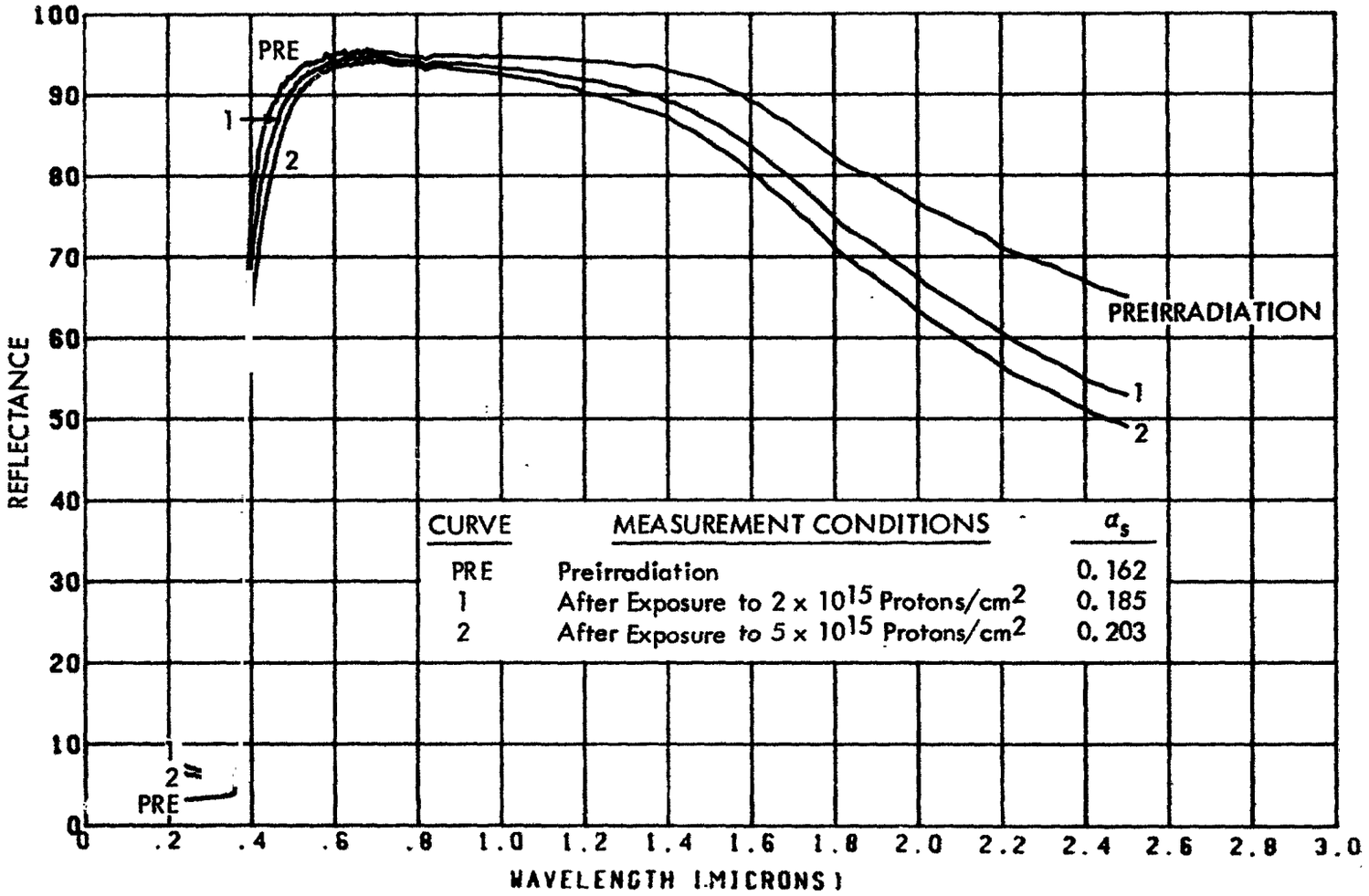

FIGURE 6.

IN SITU EFFECTS OF 1-KEV PROTONS AND THERMAL ELECTRONS ON NASA-AMES Z-93 SP-500 ZINC OXIDE PIGMENT IN POTASSIUM SILICATE 6

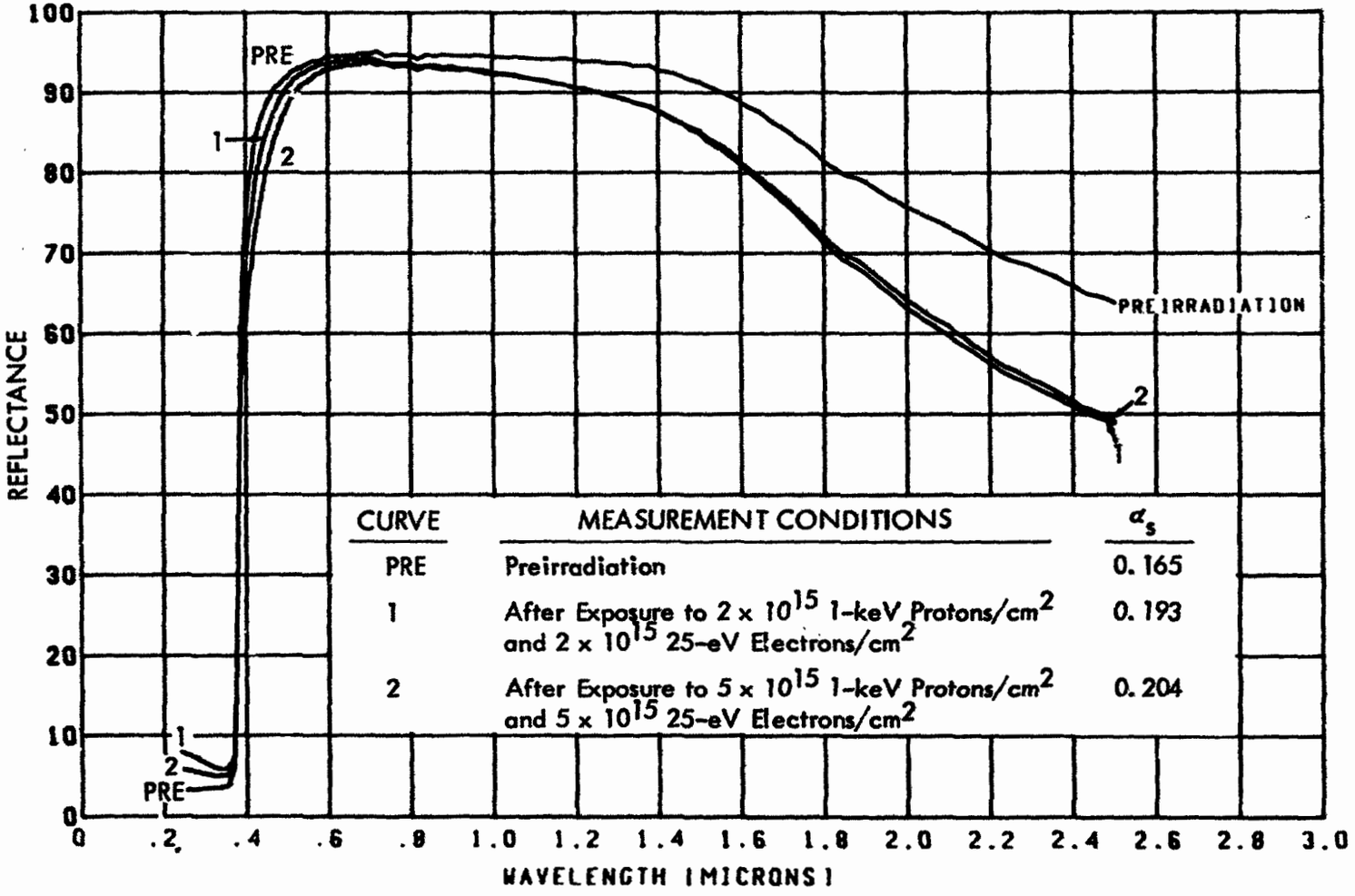

FIGURE 7. IN SITU EFFECTS OF ULTRAVIOLET RADIATION ON NASA-AMES Z-93 SP-500 ZINC OXIDE PIGMENT IN POTASSIUM SILICATE 45

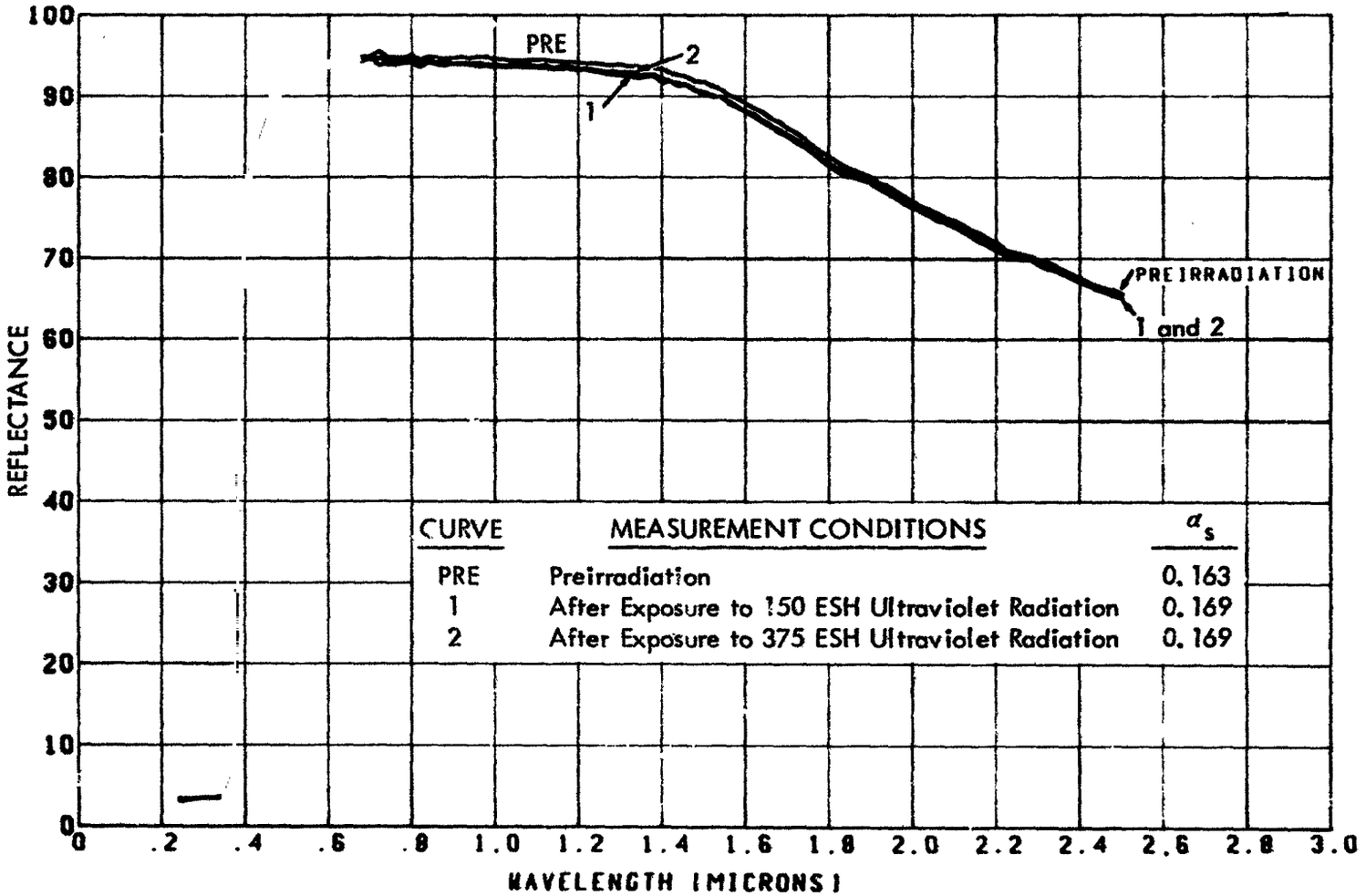

FIGURE 8.

IN SITU EFFECTS OF THERMAL ELECTRONS AND ULTRAVIOLET ON NASA-AMES Z-93 SP-500 ZINC OXIDE PIGMENT IN POTASSIUM SILICATE 33

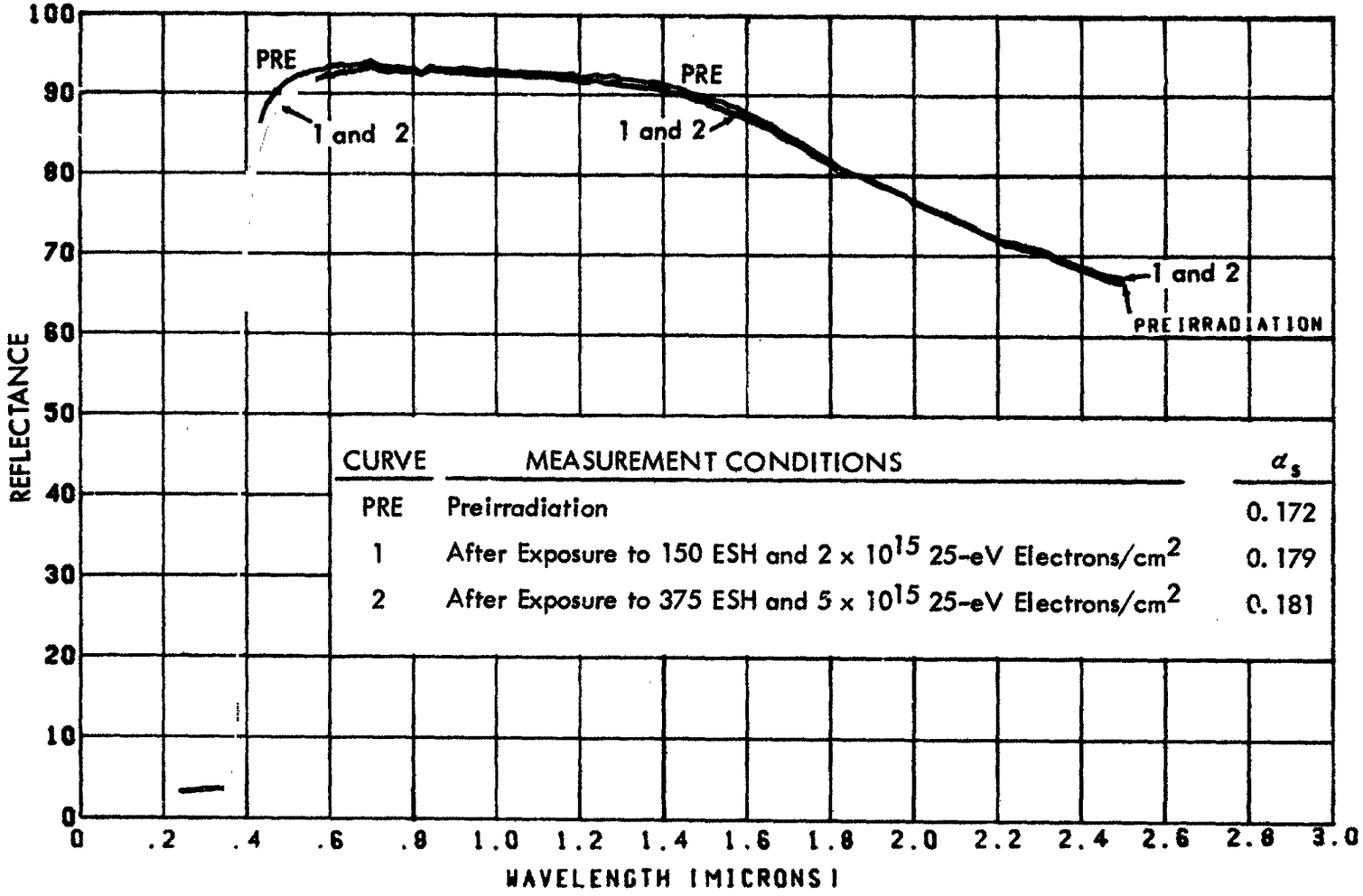

CURVE	MEASUREMENT CONDITIONS	α_s
PRE	Preirradiation	0.172
1	After Exposure to 150 ESH and 2×10^{15} 25-eV Electrons/cm^2	0.179
2	After Exposure to 375 ESH and 5×10^{15} 25-eV Electrons/cm^2	0.181

FIGURE 9.

IN SITU EFFECTS OF 1-KEV PROTONS AND ULTRAVIOLET RADIATION ON NASA-AMES Z-93 SP-500 ZINC OXIDE PIGMENT IN POTASSIUM SILICATE 7

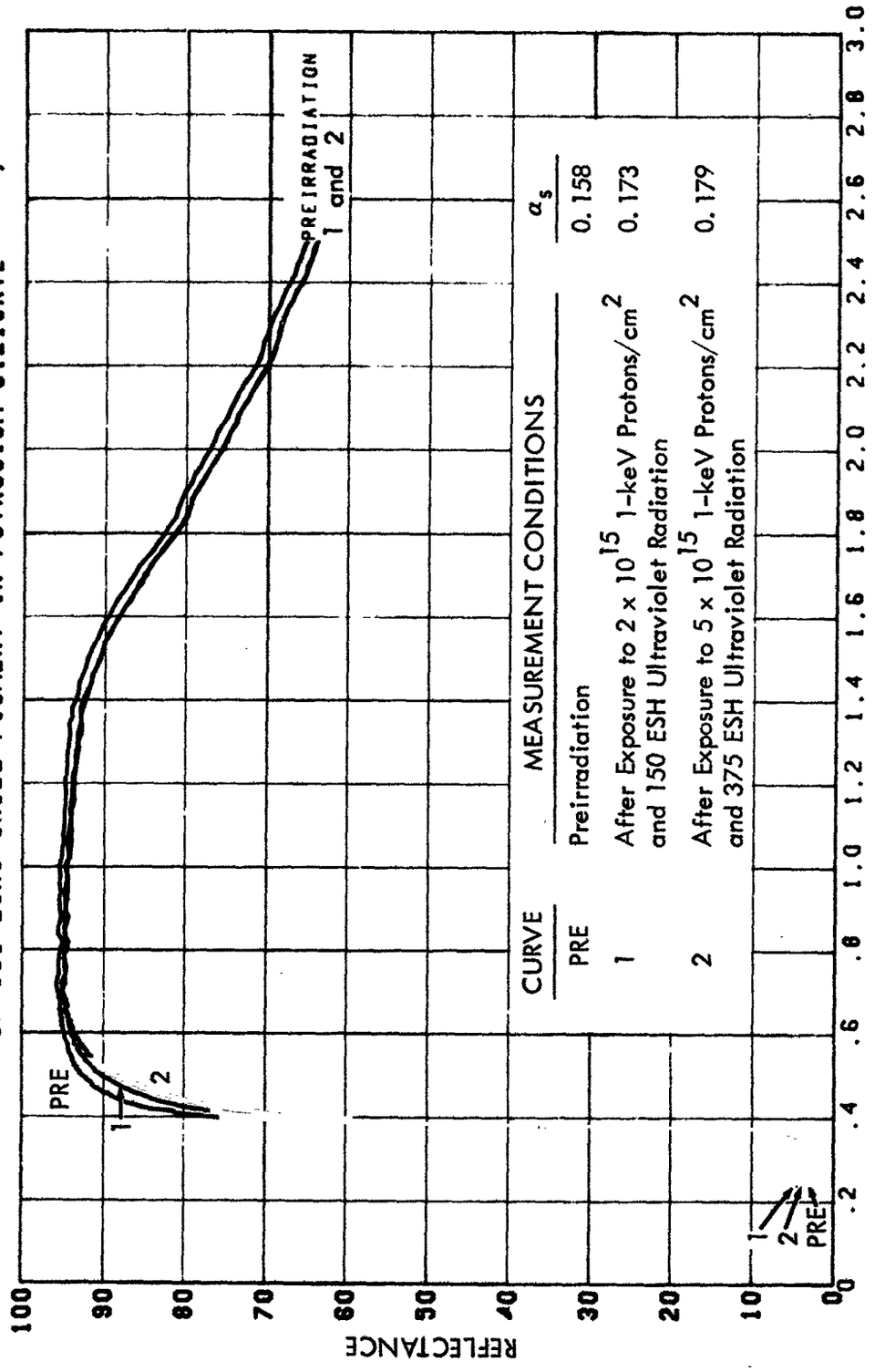

FIGURE 10. IN SITU EFFECTS OF 1-KEV PROTONS, THERMAL ELECTRONS, AND UV ON NASA-AMES Z-93 :SP-500 ZINC OXIDE PIGMENT IN POTASSIUM SILICATE 5

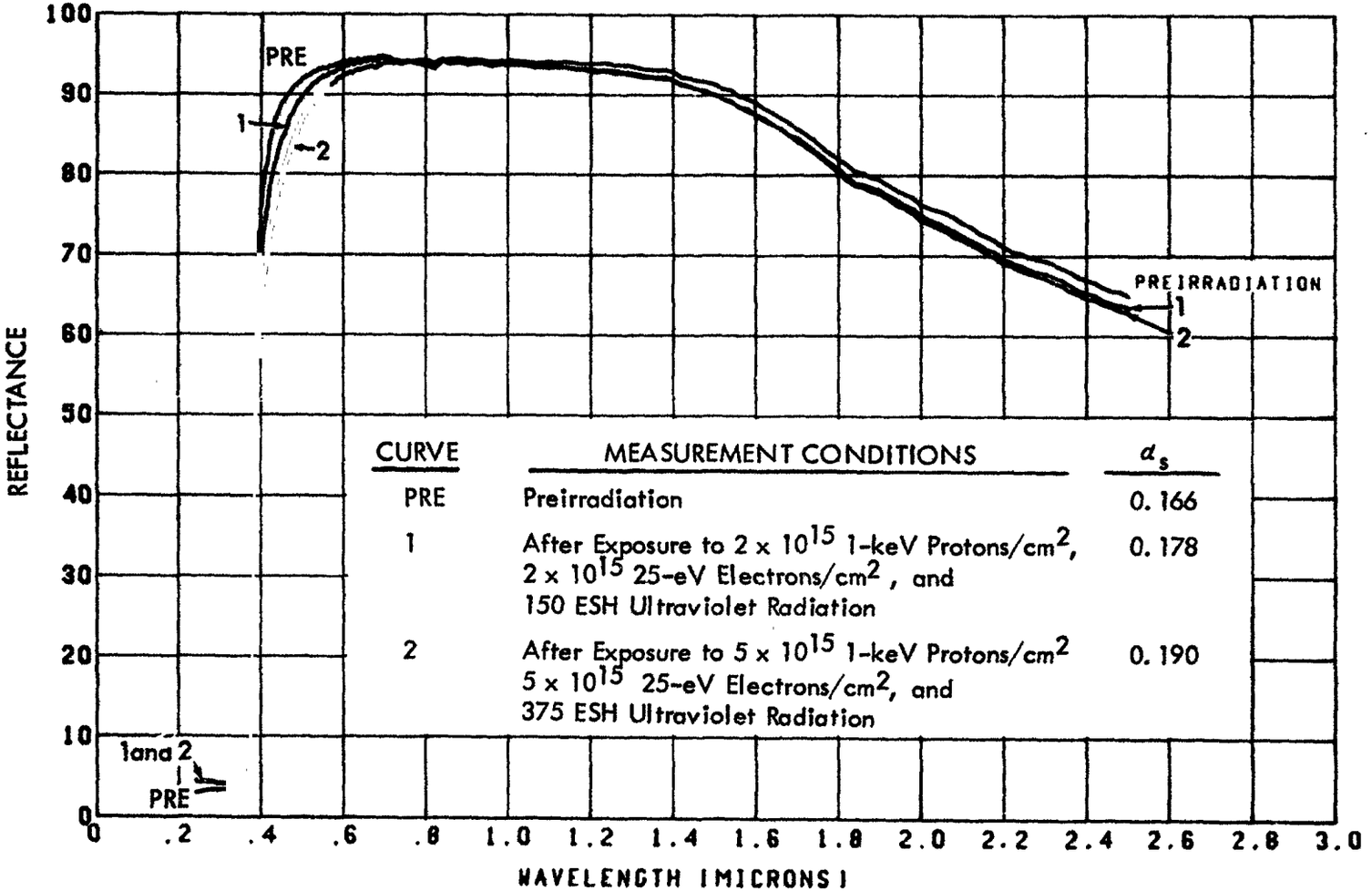

Figures 7 and 8 indicate the relative stability of Z-93's reflectance when exposed to ultraviolet radiation, alone and in combination with thermal electrons. Figures 9 and 10 present reflectance properties of Z-93 when exposed simultaneously to ultraviolet and to particle radiation. Figure 9, showing effects of protons and ultraviolet radiation on Z-93, should be contrasted with Figure 5 (proton-only exposure), which indicates lesser amounts of visible-region damage, but much greater reflectance degradation in the infrared. The "triple environment" exposure (simultaneous protons/thermal electrons/ultraviolet radiation, Figure 10) results in degradation of the same character as that indicated by Figure 9 for proton/ultraviolet exposure.

The reflectance degradation characteristics of Al_2O_3—K_2SiO_3 when exposed to the same six simulated environmental conditions are presented in Figures 11 through 16. The reflectance of Al_2O_3—K_2SiO_3 is relatively stable during proton-only and proton/thermal electron irradiation (Figures 11 and 12). Figure 13 shows the customary heavy damage Al_2O_3—K_2SiO_3 sustains at the shorter wavelengths (less than about one micron) when exposed to ultraviolet radiation. Note that reflectance degradation is almost completely saturated at 150 equivalent ultraviolet sun hours (ESH). Reflectance damage of similar spectral character but greater in extent occurs after thermal electron/ultraviolet exposure, proton/ultraviolet exposure, and proton/thermal electron/ultraviolet exposure. Results for these three types of simultaneous exposure are shown in Figures 14, 15, and 16, respectively.

Test results from additional test specimens exposed to these same simulated space radiation environmental conditions are contained in Appendix A to this report. When results indicated in Figures A-1 through A-10 are compared with the results given in Figures 5 through 16, differences in reflectance and absorptance properties are found to be within experimental precision, or may be attributed to sample-to-sample variations before exposure. In the section below, this agreement or consistency allows further analysis of visible-region reflectance changes and solar absorptance changes to be based properly on results given in Figures 5 through 16.

FIGURE 11. IN SITU EFFECTS OF 1-KEV PROTONS ON NASA-AMES AL203 ALPHA ALUMINUM OXIDE PIGMENT IN POTASSIUM SILICATE

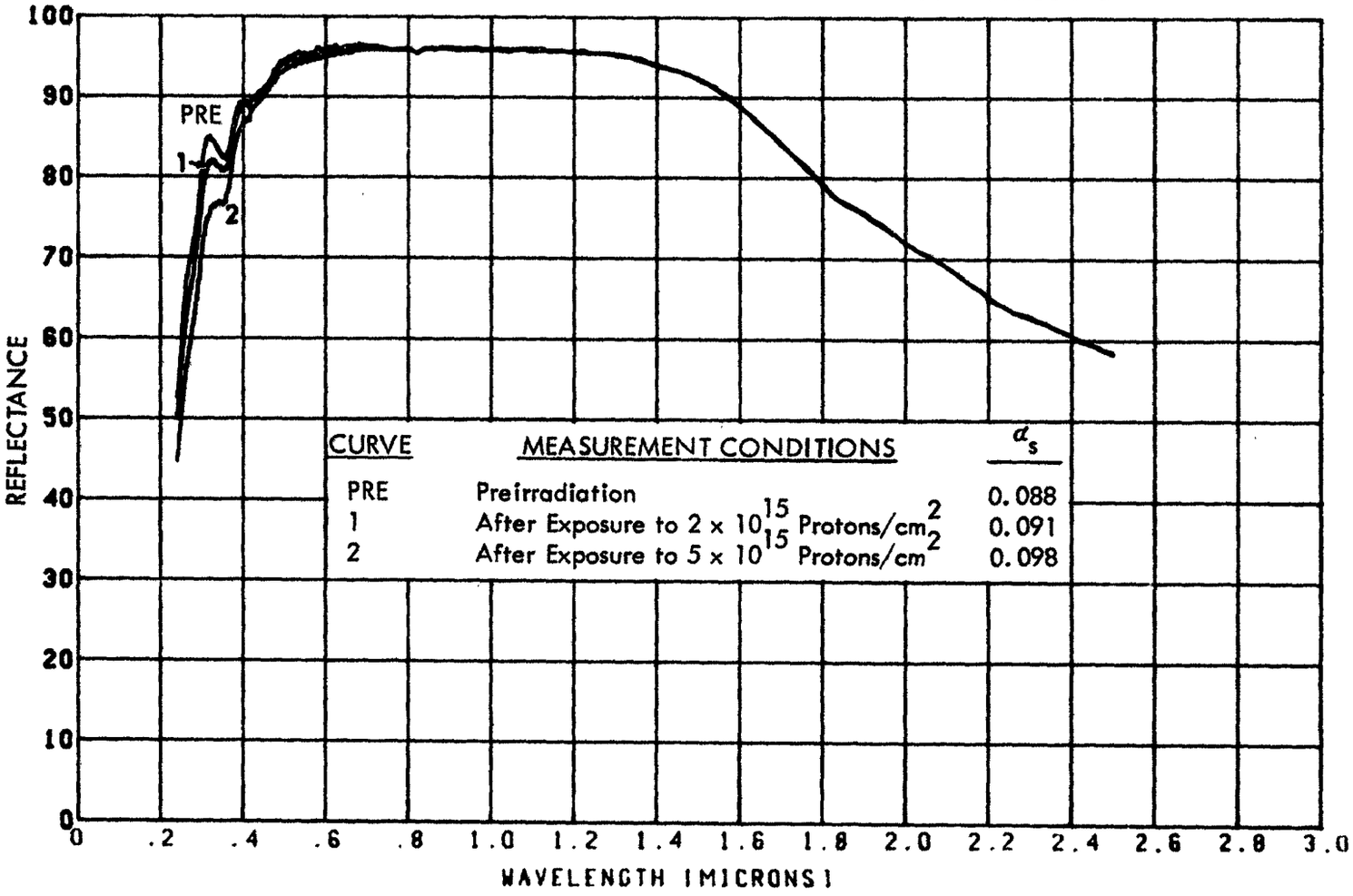

FIGURE 12. IN SITU EFFECTS OF 1-KEV PROTONS AND THERMAL ELECTRONS ON NASA-AMES AL203 ALPHA ALUMINUM OXIDE PIGMENT IN POTASSIUM SILICATE [5]

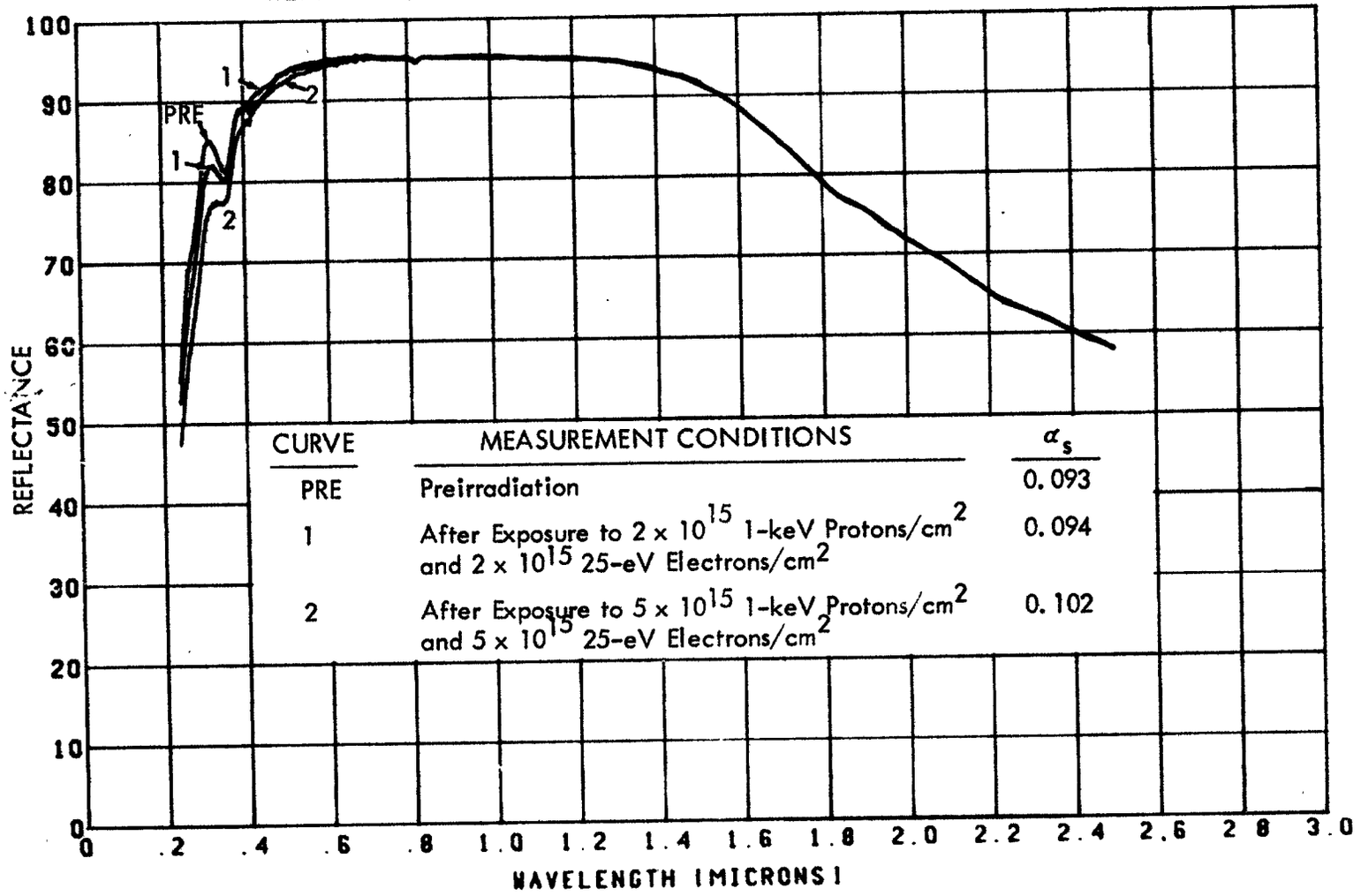

FIGURE 13. IN SITU EFFECTS OF ULTRAVIOLET RADIATION ON NASA-AMES AL203 ALPHA ALUMINUM OXIDE PIGMENT IN POTASSIUM SILICATE 70

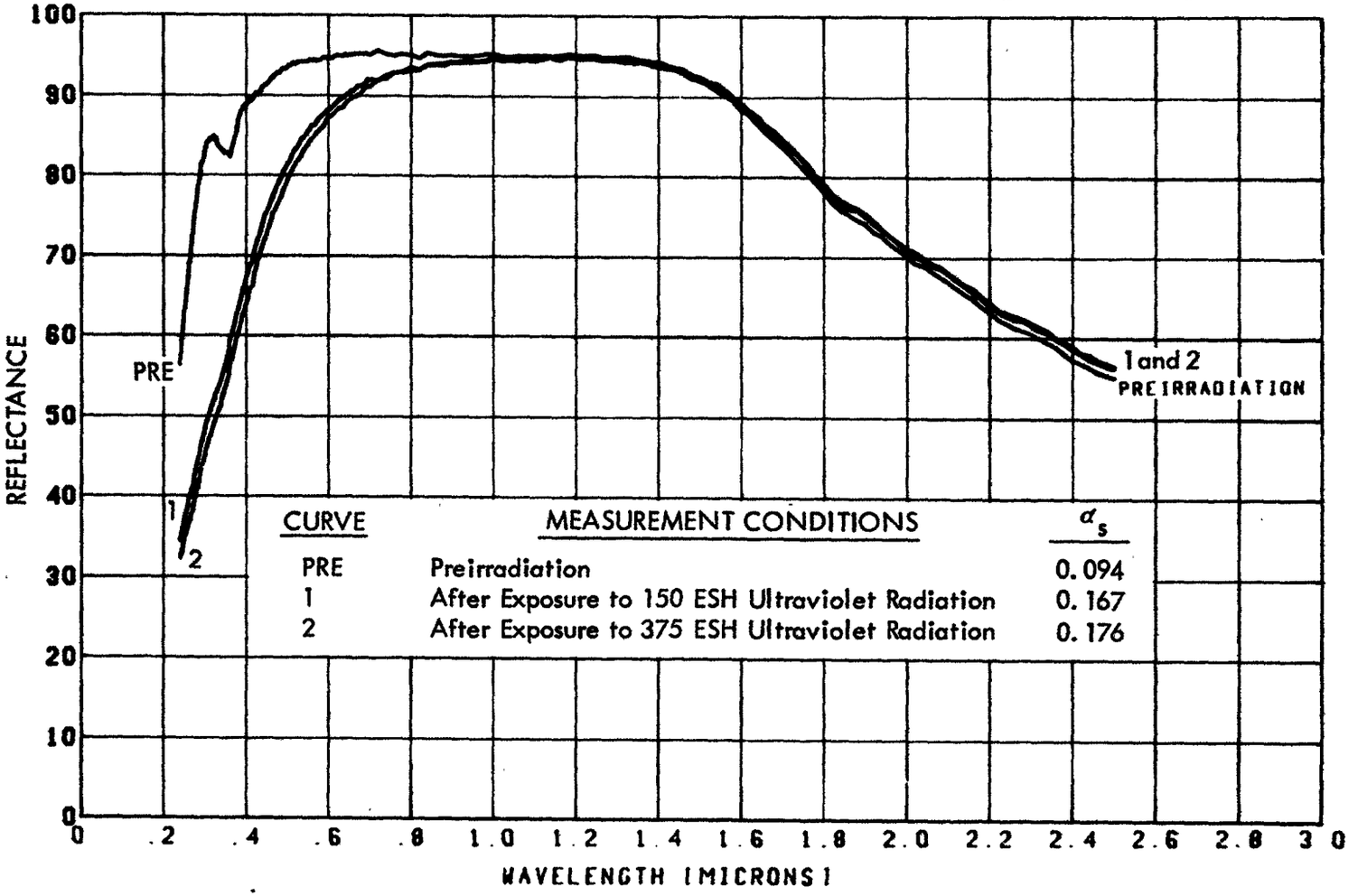

FIGURE 14. IN SITU EFFECTS OF THERMAL ELECTRONS AND ULTRAVIOLET ON NASA-AMES AL203 ALPHA ALUMINUM OXIDE PIGMENT IN POTASSIUM SILICATE 34

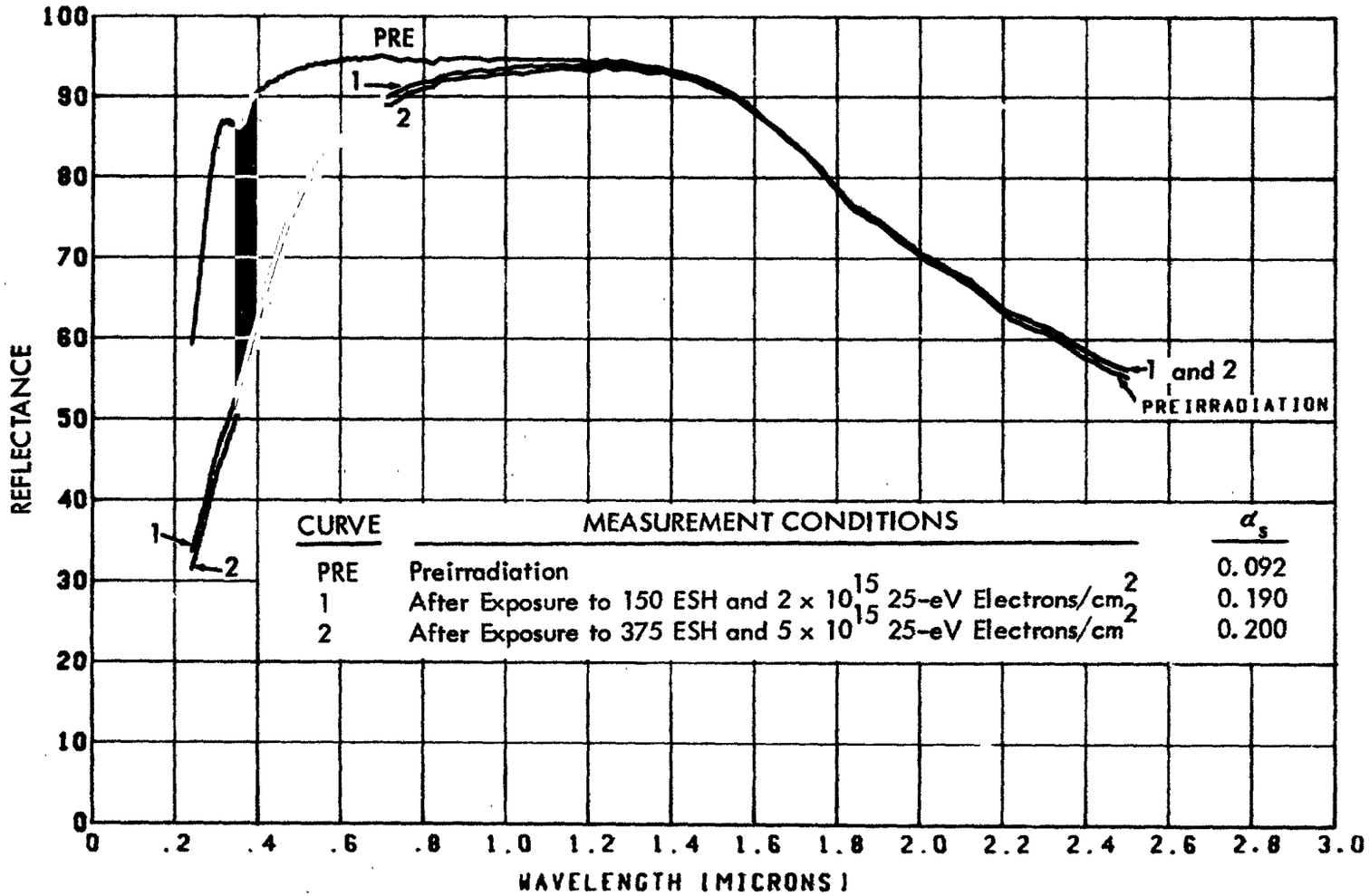

FIGURE 15. IN SITU EFFECTS OF 1-KEV PROTONS AND ULTRAVIOLET RADIATION ON NASA-AMES ALUMINUM OXIDE PIGMENT IN POTASSIUM SILICATE 10

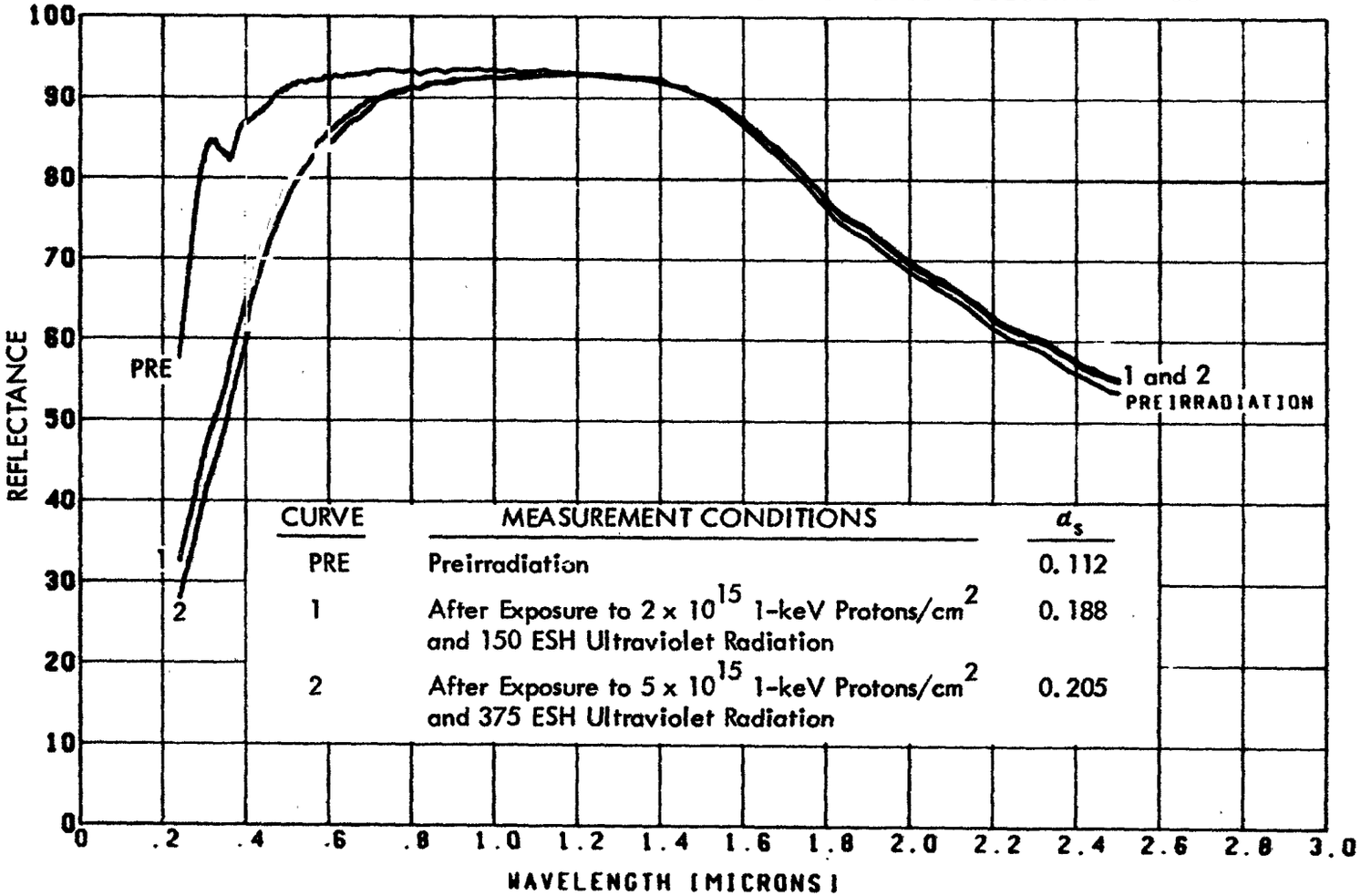

FIGURE 16.

IN SITU EFFECTS OF 1-KEV PROTONS, THERMAL ELECTRONS, AND UV ON NASA-AMES AL203 ALPHA ALUMINUM OXIDE PIGMENT IN POTASSIUM SILICATE 6

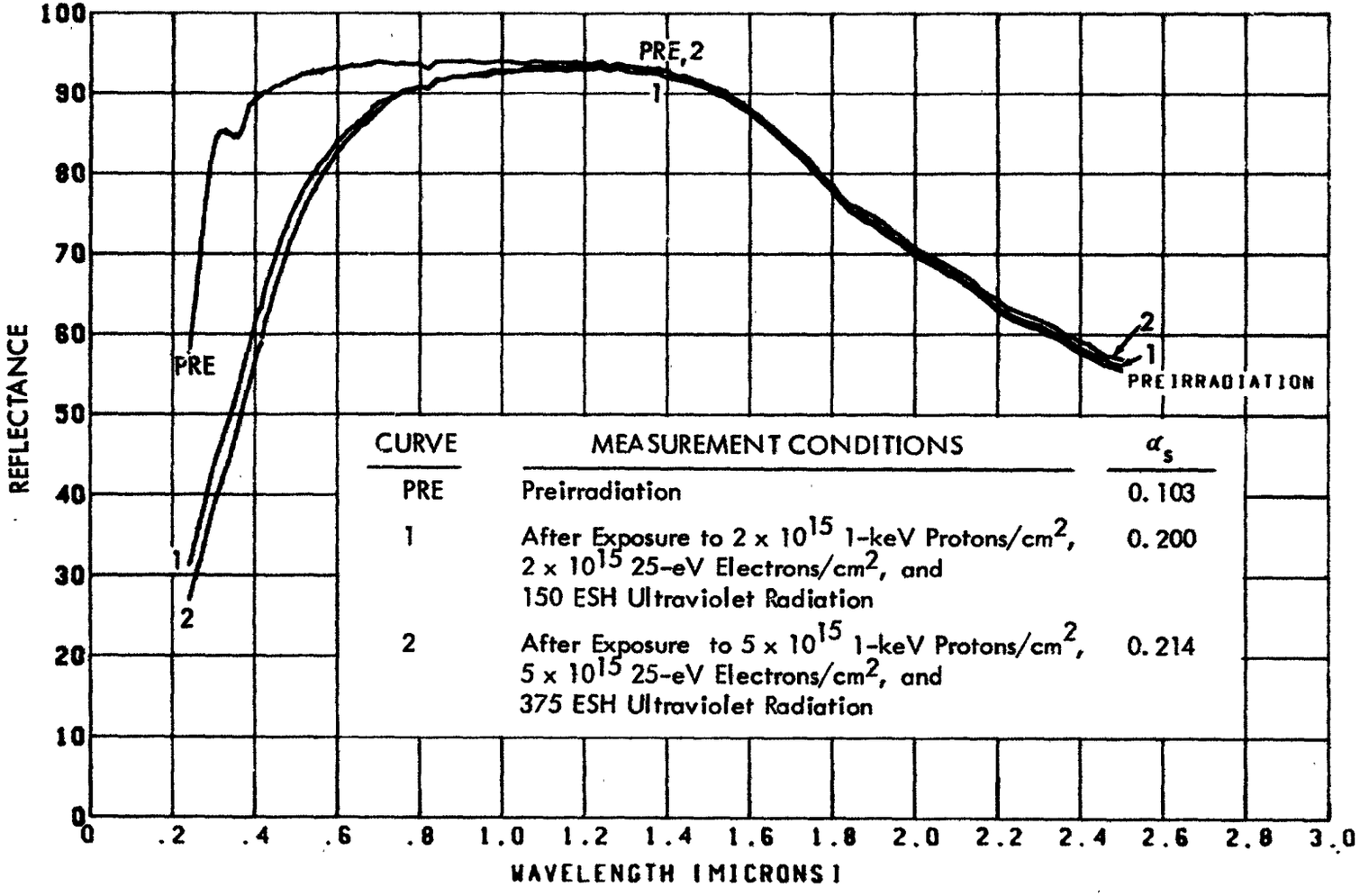

DISCUSSION AND INTERPRETATION

Reflectance Changes

An analysis of coating reflectance changes at a wavelength of 410 mμ shows the extent of degradation sustained by Z-93 and Al_2O_3—K_2SiO_3 when exposed to each of six environment combinations (Table 2). Also shown is the degree of additiveness for coating degradation at 410 mμ. The 410-mμ wavelength is representative both of the wavelength region in which the solar spectrum is most intense, and of the wavelength region in which both types of coatings are sensitive to reflectance degradation. In fact, visible-region degradation of Z-93 is a maximum at 410 mμ.

The entries in Table 2 for Z-93 confirm the results shown in reflectance vs. wavelength plots (Figures 5 through 11) — that Z-93 is damage-sensitive when exposed to particle radiation, but is quite ultraviolet-stable. Degradation of Z-93's reflectance at 410 mμ is virtually the same for the cases of proton-only and proton/thermal electron exposure. The very small reflectance changes due to exposure to ultraviolet radiation are significantly enhanced by exposure to thermal electrons and ultraviolet radiation simultaneously. In the simultaneous particle/ultraviolet exposures Z-93 again sustains significant reflectance degradation at 410 mμ. This is apparently due to the proton component of the multiple environment since there is little difference between ΔR values obtained in measurements after simultaneous proton/ultraviolet exposure and ΔR values after simultaneous proton/thermal electron/ultraviolet exposure. Finally, the smaller reflectance changes at 410 mμ observed following simultaneous proton/ultraviolet exposure, when compared with ΔR values following exposure to protons alone, suggest the existence of competing mechanisms—proton-induced atomic displacements and photon-induced "bleaching" or recovery of proton-caused damage—during simultaneous exposure.

As for additiveness of damage in Z-93, results show that reflectance degradation at 410 mμ from simultaneous proton/ultraviolet exposure is less than the sum of proton-only ΔR values and ultraviolet-only ΔR values (bottom of Table 2). Similarly, Z-93's damage from simultaneous proton/thermal electron/ultraviolet

Table 2. Analysis of Reflectance Degradation at $\lambda = 410$ mμ.

Type of Exposure	Measurement Condition	$ZnO—K_2SiO_3$ (Z-93)		$Al_2O_3—K_2SiO_3$	
		$\%\ R_{\lambda = 410\ m\mu}$	$\Delta R = R_{\lambda\ pre} - R$	$\%\ R_{\lambda = 410\ m\mu}$	$\Delta R = R_{\lambda\ pre} - R$
Protons only (1)	Preirradiation	79.2		88.8	
	After $2x10^{15}$	72.9	6.3	88.5	0.3
	After $5x10^{15}$	67.5	11.7	86.9	1.9
Simultaneous protons and thermal electrons (2)	Preirradiation	79.1		89.0	
	After $2x10^{15}$	73.2	5.9	89.1	-0.1
	After $5x10^{15}$	67.0	12.1	87.4	1.6
Ultraviolet only (3)	Preirradiation	80.2		89.3	
	After 150 ESH	80.2	0.0	69.3	20.0
	After 375 ESH	79.7	0.5	65.8	23.5
Simultaneous ultraviolet and thermal electrons (4)	Preirradiation	79.9		90.7	
	$150/2x10^{15}$	77.4	2.5	64.3	26.4
	$375/5x10^{15}$	77.2	2.7	62.2	28.5
Simultaneous protons and ultraviolet (5)	Preirradiation	80.8		87.1	
	$2x10^{15}/150$	75.6	5.2	67.0	20.1
	$5x10^{15}/375$	70.8	10.0	61.8	25.3
Simultaneous protons, thermal electrons, and ultraviolet (6)	Preirradiation	80.4		89.2	
	$2x10^{15}/150$	74.1	6.3	62.9	26.3
	$5x10^{15}/375$	68.0	12.4	58.4	30.8

Σ(1) & (3) compare with (5)	After $2x10^{15}$ and 150 ESH	6.3	20.3
	After $5x10^{15}$ and 375 ESH	12.2	25.4
Σ(1) & (4) compare with (6)	After $2x10^{15}$ and 150 ESH	8.8	26.7
	After $5x10^{15}$ and 375 ESH	14.4	30.4
Σ(2) & (3) compare with (6)	After $2x10^{15}$ and 150 ESH	5.9	19.9
	After $5x10^{15}$ and 375 ESH	12.6	25.1

exposure is less than the sum of ΔR values taken from proton-only exposure and ultraviolet/thermal electron exposure. However, proton/thermal electron/ultraviolet damage at 410 mμ is virtually equal to the sum of ΔR values from ultraviolet-only exposure and proton/thermal electron exposure.

Reflectance degradation of the aluminum oxide—potassium silicate coating at 410 mμ is found to be additive (within experimental error) in two cases of multiple environment exposure, and significantly greater than additive in a third case. For example, reflectance changes after proton-only exposure and after ultraviolet-only exposure when summed are nearly equal to the amount of degradation sustained by Al_2O_3—K_2SiO_3 when exposed simultaneously to protons and ultraviolet radiation. When ΔR values obtained after proton-only exposure are added to ΔR values due to simultaneous ultraviolet/thermal electron exposure, the results agree quite favorably with ΔR values sustained by Al_2O_3—K_2SiO_3 in simultaneous proton/thermal electron/ultraviolet exposure. However, if ΔR values from simultaneous proton/thermal electron exposure are added to the amounts of degradation at 410 mμ due to exposure to ultraviolet radiation alone, and then compared with ΔR values sustained during simultaneous proton/thermal electron/ultraviolet exposure, the latter values are some 20 percent greater than the arithmetic sum. This is a case of greater-than-additive degradation occurring in multiple environment exposure. These contrasting results, valid both for Al_2O_3—K_2SiO_3 and for Z-93, demonstrate that thermal electrons contribute to more reflectance damage when combined with ultraviolet radiation than when combined with 1-keV protons.

It is also observed in the case of aluminum oxide—potassium silicate that ΔR values for proton-only exposure and for proton/thermal electron exposure agree within experimental error, again indicating that thermal electrons do not contribute materially to visible-region reflectance damage when combined with protons in particle-only exposure. On the other hand, Table 2 shows that the combination of thermal electrons and ultraviolet results in significantly greater reflectance degradation in Al_2O_3—K_2SiO_3 at 410 mμ than does exposure to ultraviolet radiation alone. Similarly, the proton/thermal electron/ultraviolet combination of radiation exposure yields larger reflectance changes than does proton/ultraviolet exposure.

Both cases illustrate the contribution to damage caused by the combination of ultraviolet and thermal electron exposure.

Solar Absorptance

A weighting of the reflectance degradation characteristics of Z-93 and Al_2O_3—K_2SiO_3 relative to electromagnetic energy emitted by the sun provides an assessment of the performance of each coating as a solar reflector or absorber. Solar absorptance (α_s) numbers on a scale from zero (no coating absorption) to unity (total absorption of incident energy) are included in Figures 5 through 16 and in Figures A-1 through A-10 for each type of radiation exposure. Derivation of each solar absorptance decimal is based upon the equation

$$\alpha_s = 1 - R_s = 1 - \frac{\int R_c(\lambda)\, I_s(\lambda)\, d\lambda}{\int I_s(\lambda)\, d\lambda}$$

where $R_c(\lambda)$ is coating reflectance as a function of wavelength, $I_s(\lambda)$ is solar irradiance as a function of wavelength, and thus R_s is a solar reflectance value weighted according to air-mass-zero (space) solar intensity across a given wavelength region of interest. For thermal control evaluation purposes, more than 97 percent of solar electromagnetic energy is included by integrating between wavelength limits of $\lambda = 0.25\ \mu$ and $\lambda = 2.50\ \mu$. In practice it is common to substitute summation of coating reflectance values at chosen discrete wavelengths ($R_{c,\lambda}$) and make use of the fact that $\int I_s(\lambda)\, d\lambda$ = solar constant. Then

$$\alpha_s = 1 - R_s = 1 - \frac{\sum R_{c,\lambda} I_\lambda}{\text{solar constant}} .$$

Further simplification is provided by choosing wavelengths that are themselves weighted against the solar spectral intensity. If, for example, the solar spectrum is divided into 100 wavelength bands each with one percent of total solar energy, and coating reflectance determined at the mid-point of each band ($R_{c\lambda}$), then

$$\alpha_s = 1 - R_s = 1 - \frac{\sum_{100} R_{c\lambda}}{100}$$

(The denominator is 100 if reflectance is on a decimal scale from zero to unity; it is 10^4 if reflectance numbers are scaled from zero to 100).

What is found for both types of coatings studied [ZnO—K_2SiO_3 (Z-93) and Al_2O_3—K_2SiO_3] is that the addition of thermal electrons to other components of the simulated solar wind environment nearly always results in the measurement of greater increase in solar absorptance values with exposure. Figures 17 and 18 show this effect and the general effect of increasing the complexity of environmental exposure simulation. With the exception of particle-only exposure of Z-93, the tendency to measure more damage in Z-93 when more components of the solar wind environment are simulated in the laboratory, is apparent in Figure 17. (It should be noted that the vertical scale of Figure 17 is expanded greatly, relative to that of Figure 18, to separate the display of data; consequently, all three cases of crossover in the data between the lower and upper exposure levels are at the edge of experimental accuracy.) The experimental results at the lower exposure level in Figure 17 and 18 may be compared with data obtained in an earlier exploratory program reported in Reference 9 and discussed in Appendix B. The results for Al_2O_3—K_2SiO_3 (Figure 18) are more orderly, with the "triple-environment" (p/e/uv) simulated exposure indicating the greatest solar absorptance damage (within experimental error). This trend in the program results is in the direction of resolving the widely noted discrepancy between (1) large buildup of values of the ratio of coating solar absorptance to emittance (α_s/ϵ), as indicated by temperature readings during space flights, and (2) lesser amounts of damage measured after laboratory-simulated exposures.

The scope of this program has not permitted a study of possible effects of other "thermal" or low energy electron sources in the environmental chamber upon exposure results. It is certainly possible for electrostatic field lines in some chamber configurations to allow electrons to stream from any thermionic electron source (such as a hot-filament ionization gauge) to dielectric materials such as white-pigmented thermal control coating samples, when those samples possess a net positive charge. The possibility then arises that any proton exposure is

FIGURE 17. INCREASE IN Z-93 SOLAR ABSORPTANCE AS A FUNCTION OF EXPOSURE

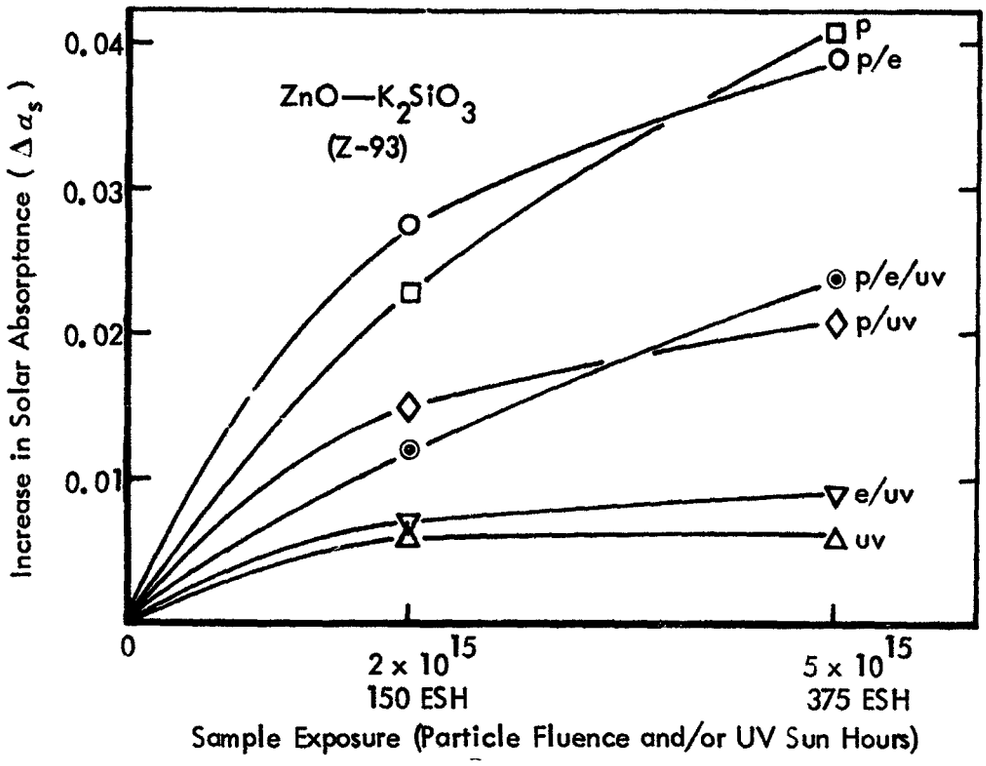

FIGURE 18. INCREASE IN Al_2O_3—K_2SiO_3 SOLAR ABSORPTANCE AS A FUNCTION OF EXPOSURE

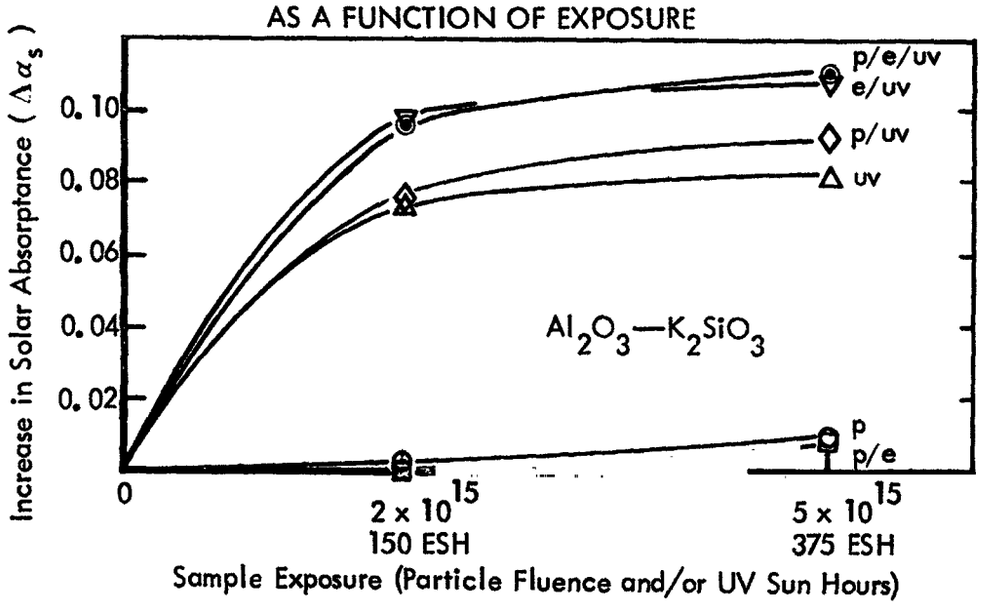

accompanied by neutralization with electrons from some "virtual" electron source. In this program a hot-filament ionization gauge has been used to monitor chamber vacuum levels during all exposures. Chamber configuration is such that field lines from gauge to samples would take a very tortuous path. Whether, then, low energy electrons from a virtual source have contributed to reflectance changes observed during all exposures conducted for this program is uncertain. What is clearly known is that experimental differences in sample reflectance properties are measured when samples are intentionally exposed to thermal electrons.

In-Vacuum Reflectance Recovery

The stability of measured spectral reflectance has been checked for selected proton-irradiated specimens remaining in a 10^{-8} torr vacuum over a period of more than 2 days following exposure. Results indicate that the reflectance of Al_2O_3—K_2SiO_3 is stable to within 0.5 percent throughout the 0.24- to 2.5-micron wavelength region measured. The spectral reflectance of ZnO—K_2SiO_3 (Z-93) is even more stable at wavelengths in the visible region, but improves slowly with time in dark, 10^{-8} torr vacuum in the infrared wavelength region (Figure 19). This recovery is significant because, like proton-induced degradation, it increases in extent with increasing wavelength. This suggests that important information about coating reflectance and emittance properties would become known by measuring further into the infrared wavelength region (beyond the current limit of about 2.5 microns). Such measurements, in fact, may be expected to contribute significantly to resolving the discrepancy between space flight and laboratory data. With this present contribution regarding the role of thermal electrons in causing coating reflectance damage, the discrepancy has been reduced but not eliminated. To date, analyses of space flight α_s/ϵ ratio data generally have assumed a space-stable ϵ with changing α_s. But this assumption has been based primarily upon the availability of vacuum (in situ) α_s data and in-air ϵ data. Figures 5, 6, and 19 add to the growing body of knowledge (such as Reference 10) that suggests significant in situ emittance changes are caused by particle exposure. Indeed there does exist information about subtle emittance changes as measured in air (Reference 11, for example). Remem-

FIGURE 19.

IN-VACUUM REFLECTANCE RECOVERY AFTER PROTON EXPOSURE OF NASA-AMES Z-93: SP-500 ZINC OXIDE PIGMENT IN POTASSIUM SILICATE

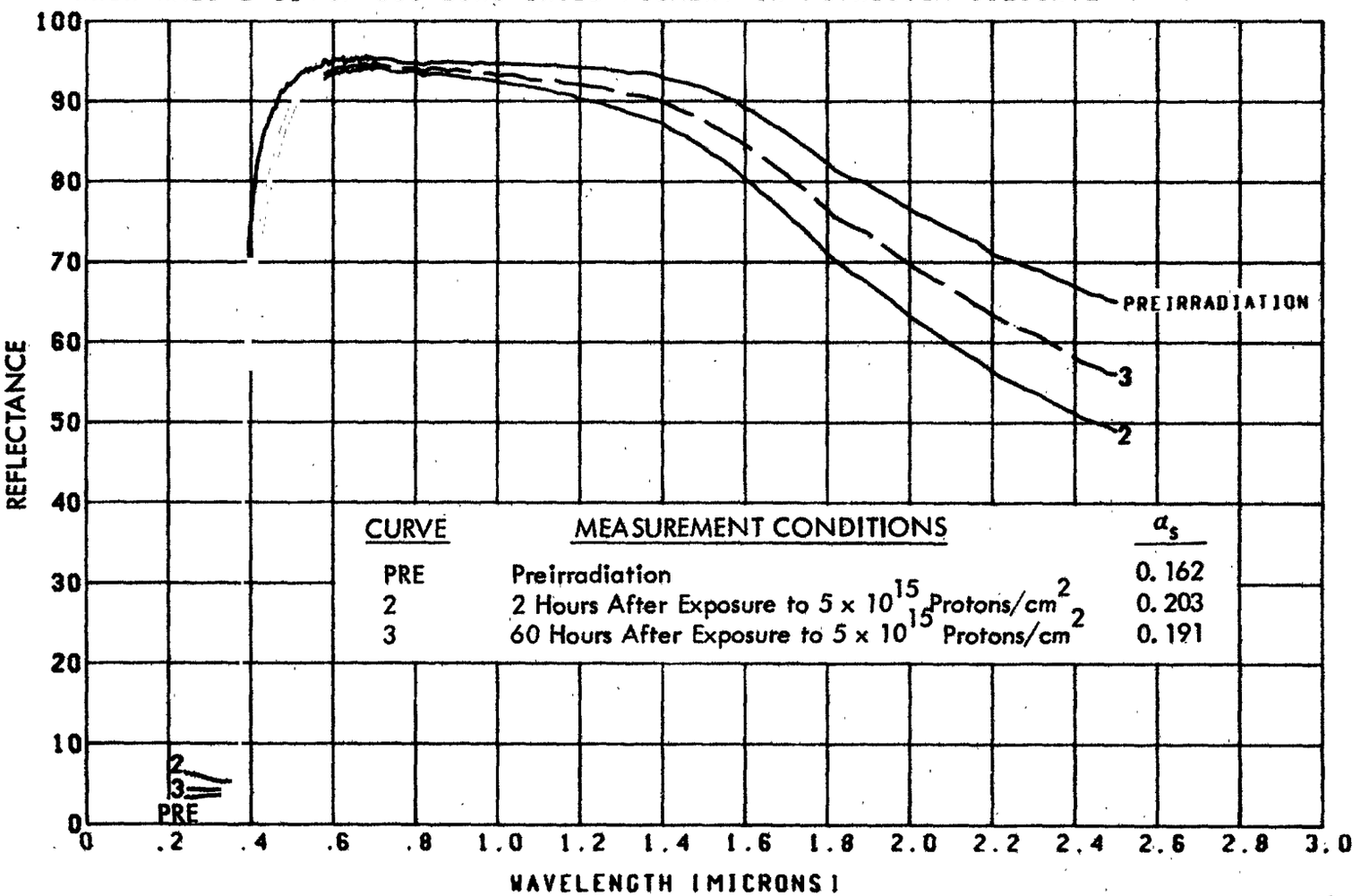

bering the observance of the dramatic "in situ effect" in 1965 (in the α_s region), these more recent results using advances in simulation technology should be sufficient incentive for extension of in situ measurements to longer wavelengths.

CONCLUSIONS AND RECOMMENDATIONS

The experimental results of this program are consistent enough to lead to definite conclusions and recommendations for future work to resolve remaining discrepancies between space and ground (laboratory) radiation effects data.

Conclusions

- The addition of 25-eV "thermal" electrons to other components of the space radiation environment (solar wind protons, and solar ultraviolet and longer wavelength radiation, separately or together) results in a preponderance of somewhat greater measured reflectance degradation of two currently-used spacecraft thermal control coatings, Z-93 and Al_2O_3—K_2SiO_3. The damage is not enough greater, however, to account for the observed discrepancy between space flight α_s/ϵ (solar absorptance/emittance) ratio data, and α_s values determined by laboratory simulation.

- Synergistic effects—differences in the magnitude of effects of multi-environment radiation exposure from predictions based upon the arithmetic sum of effects of single-environment exposures—exist in the coatings studied for this program. Most notable is the near-cancellation of proton-induced infrared-region damage in Z-93 by the addition of ultraviolet and longer wavelength photon radiation in simultaneous exposure with protons. This implies a photon-induced reflectance recovery mechanism successfully competing with the proton-induced damage mechanism.

- Reflectance changes which increase with wavelength, and reflectance recovery with time in vacuum following proton exposure, both imply that coating emittance as well as absorptance is affected by radiation exposure.

Recommendations

This program should be followed by:

- further improvements in the completeness of space radiation environmental simulation in the laboratory. Included should be exploratory exposure of the same thermal control coatings to neutral hydrogen (molecular or monatomic), thermal electrons alone, alpha particles, combined protons and alpha particles, and combinations of the last two with solar electromagnetic radiation (ultraviolet and longer wavelengths).

- the establishment of capability to measure coating thermal emittance in vacuum (in situ) following particle and ultraviolet radiation exposure. It is believed that this is the next most plausible step to take to achieve agreement between laboratory predictions and space flight data.

APPENDIX A

ADDITIONAL EXPERIMENTAL RESULTS

Experimental data for most environmental exposure conditions simulated is available from more than one thermal control coating sample of each type studied. Reflectance vs. wavelength plots of data from these additional (or mulitplicity) samples are contained in this Appendix (Figures A-1 through A-10) as an indication of the consistency of the experimental results obtained.

Results of in-air measurements on two selected coating specimens are presented in Figures A-11 and A-12. Four curves relate reflectance versus wavelength for the conditions of (1) in air before chamber pumpdown and radiation exposure; (2) in vacuum before radiation exposure; (3) in vacuum after exposure to 375 ESH ultraviolet radiation; and (4) in air after chamber backfill. The differences in reflectance properties as measured in air and in vacuum (in situ) are evident.

FIGURE A-1.

IN SITU EFFECTS OF 1-KEV PROTONS ON NASA-AMES Z-93
SP-500 ZINC OXIDE PIGMENT IN POTASSIUM SILICATE

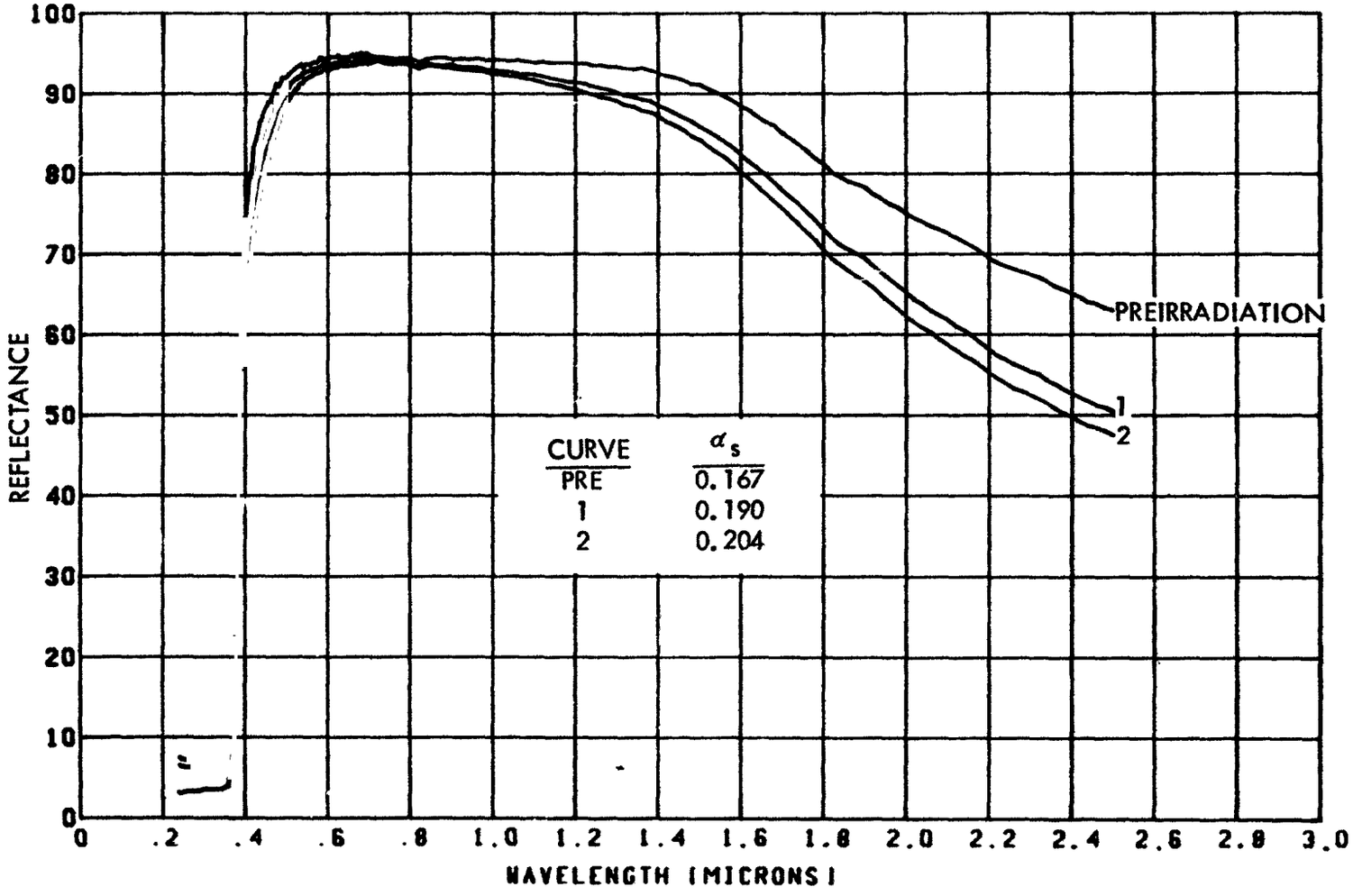

FIGURE A-2.

IN SITU EFFECTS OF 1-KEV PROTONS AND THERMAL ELECTRONS ON NASA-AMES Z-93 SP-500 ZINC OXIDE PIGMENT IN POTASSIUM SILICATE 4

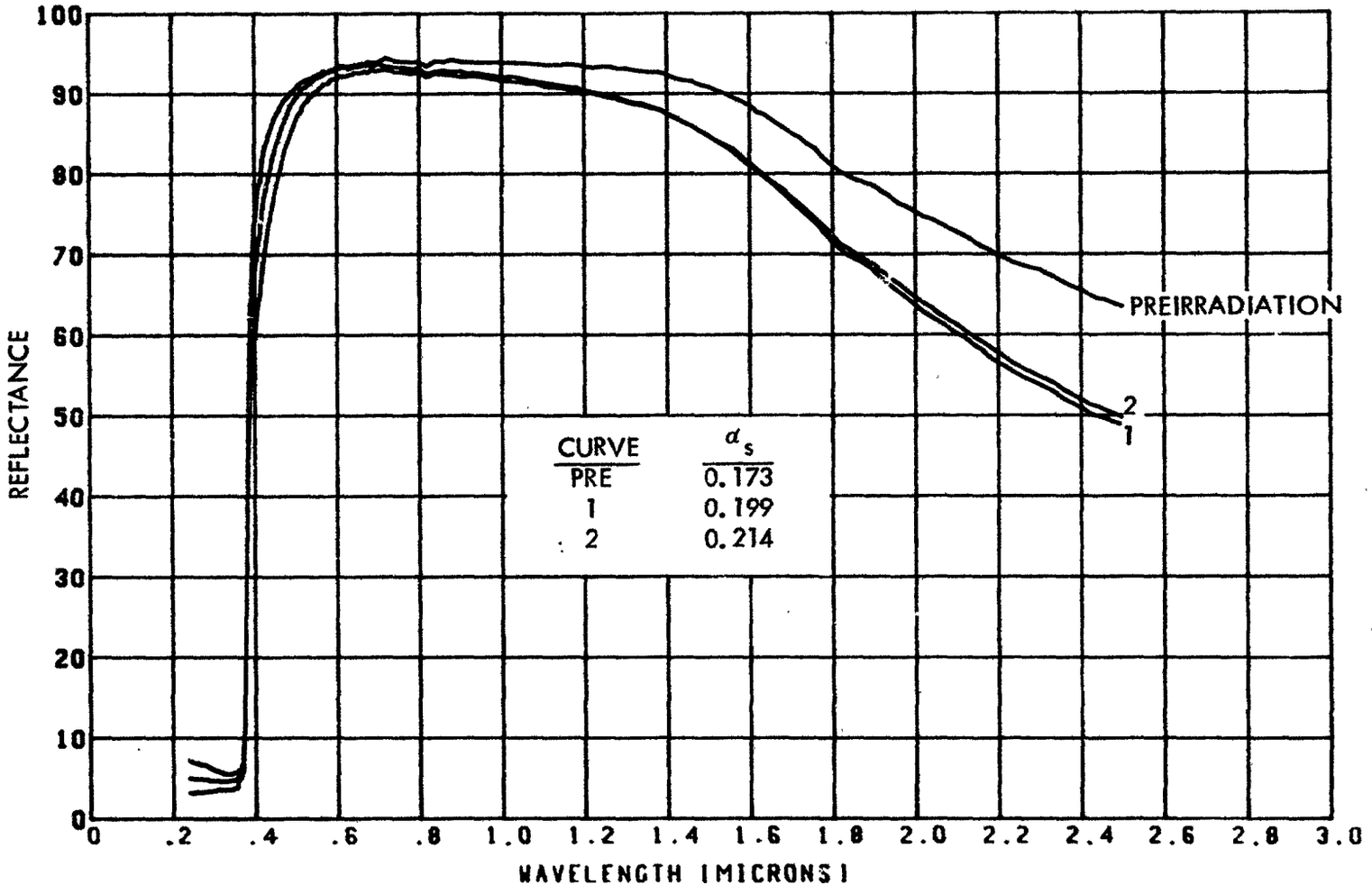

FIGURE A-3.

IN SITU EFFECTS OF THERMAL ELECTRONS AND ULTRAVIOLET ON NASA-AMES Z-93 SP-500 ZINC OXIDE PIGMENT IN POTASSIUM SILICATE 50

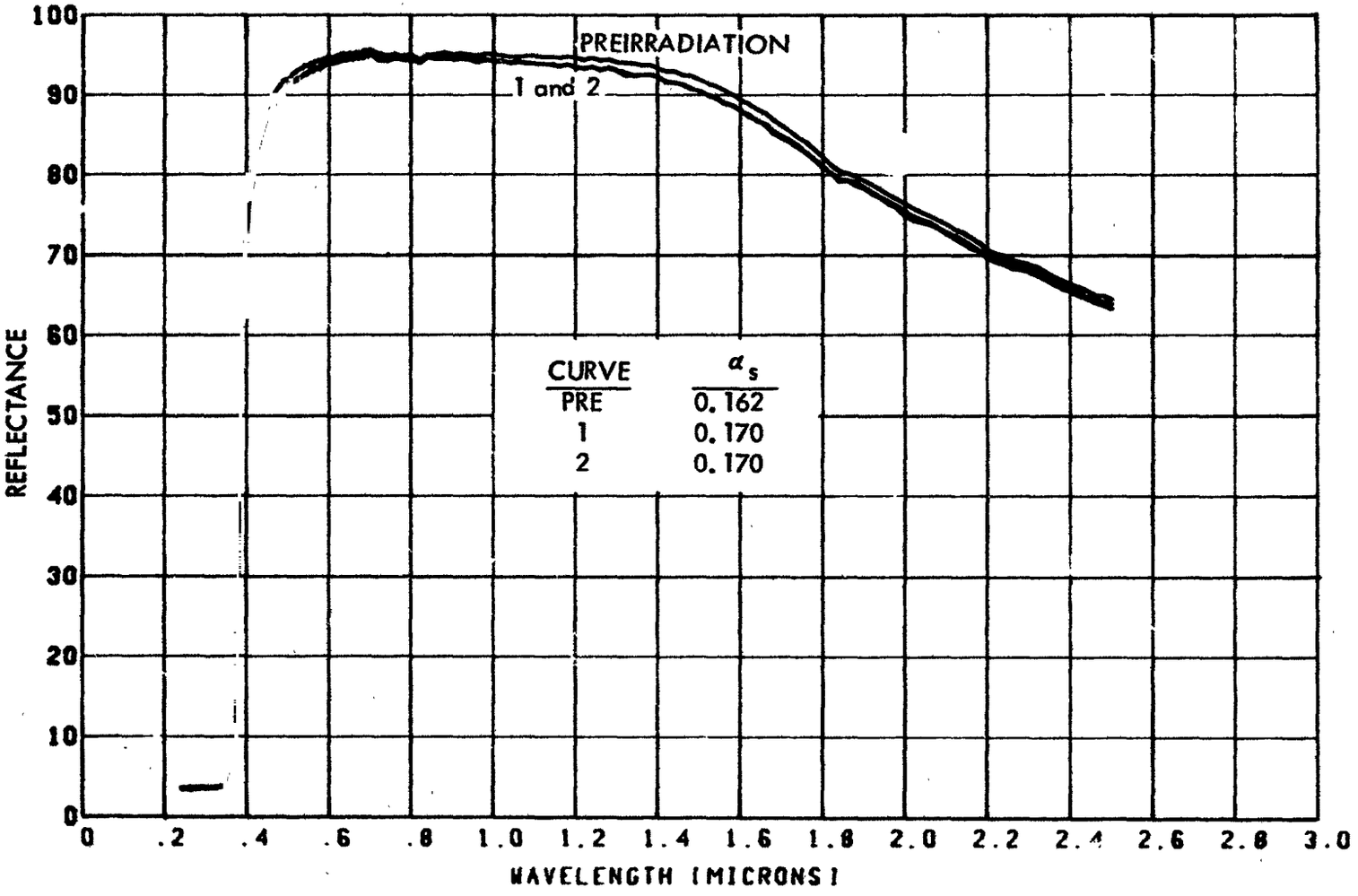

FIGURE A-4.

IN SITU EFFECTS OF 1-KEV PROTONS AND ULTRAVIOLET RADIATION ON NASA-AMES Z-93 SP-500 ZINC OXIDE PIGMENT IN POTASSIUM SILICATE 11

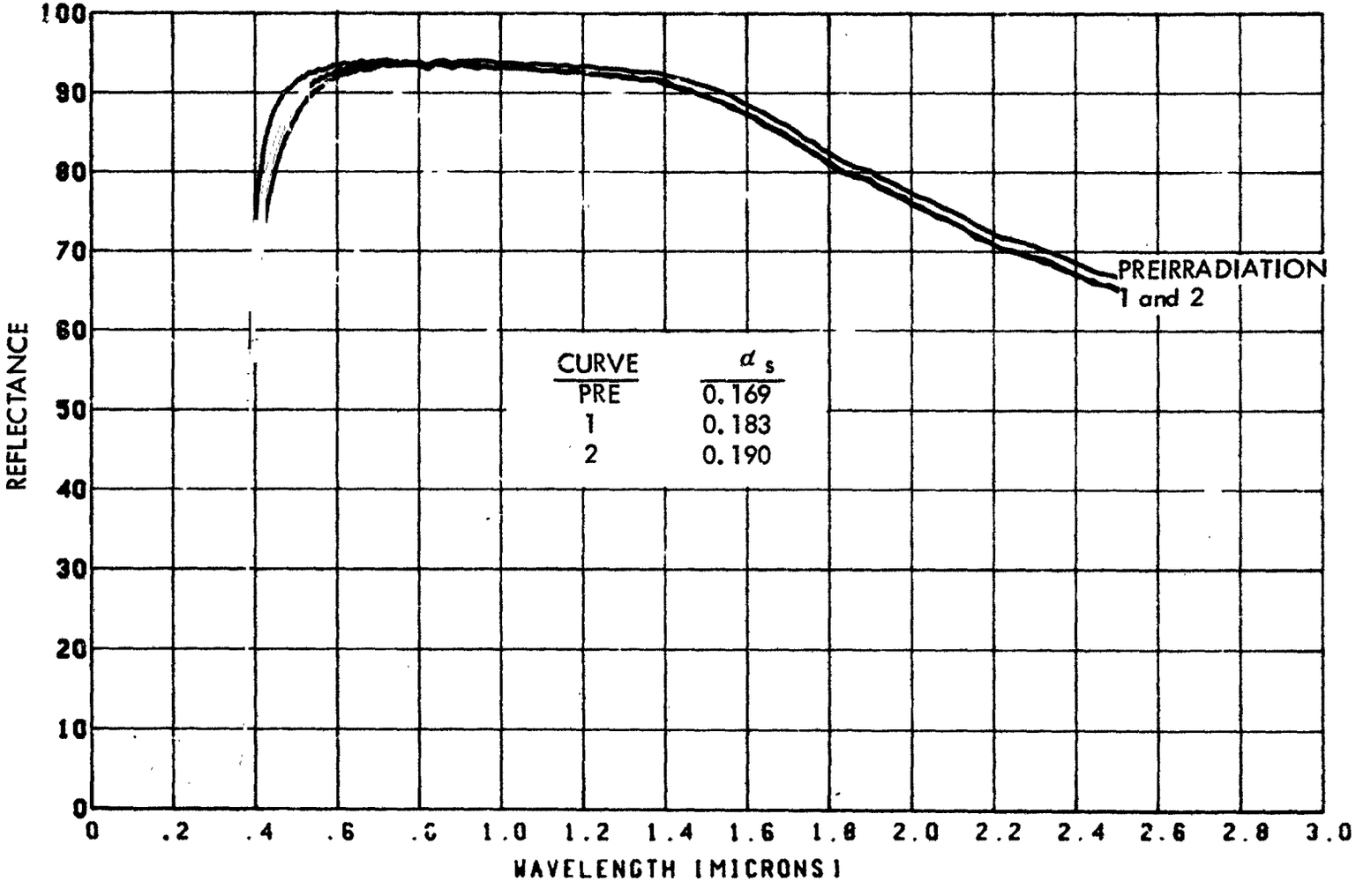

FIGURE A-5.

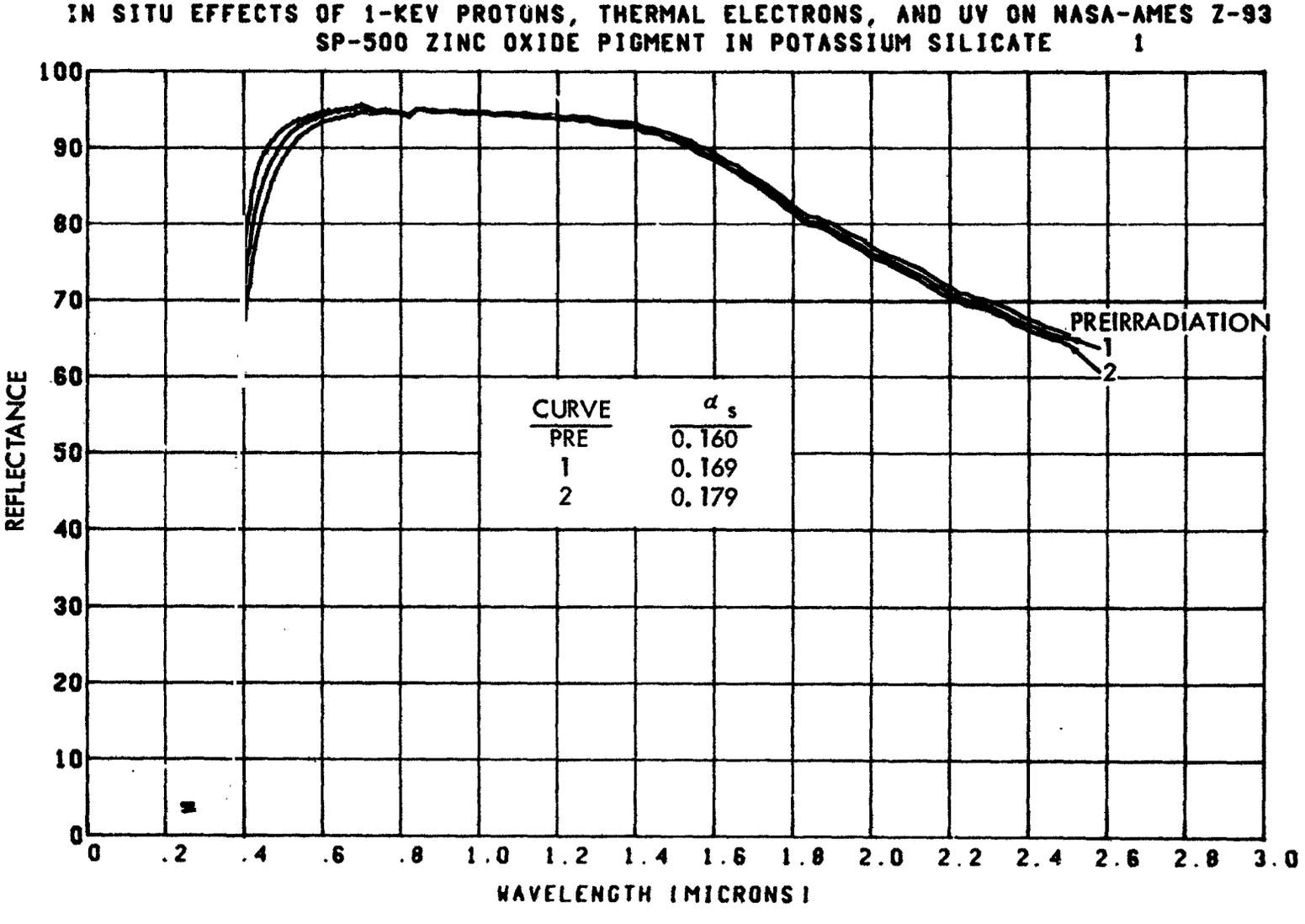
IN SITU EFFECTS OF 1-KEV PROTONS, THERMAL ELECTRONS, AND UV ON NASA-AMES Z-93
SP-500 ZINC OXIDE PIGMENT IN POTASSIUM SILICATE 1
REFLECTANCE
WAVELENGTH (MICRONS)
PREIRRADIATION
1
2
CURVE
PRE
1
2
α_s
0.160
0.169
0.179

FIGURE A-6.

IN SITU EFFECTS OF 1-KEV PROTONS ON NASA-AMES AL_2O_3 ALPHA ALUMINUM OXIDE PIGMENT IN POTASSIUM SILICATE

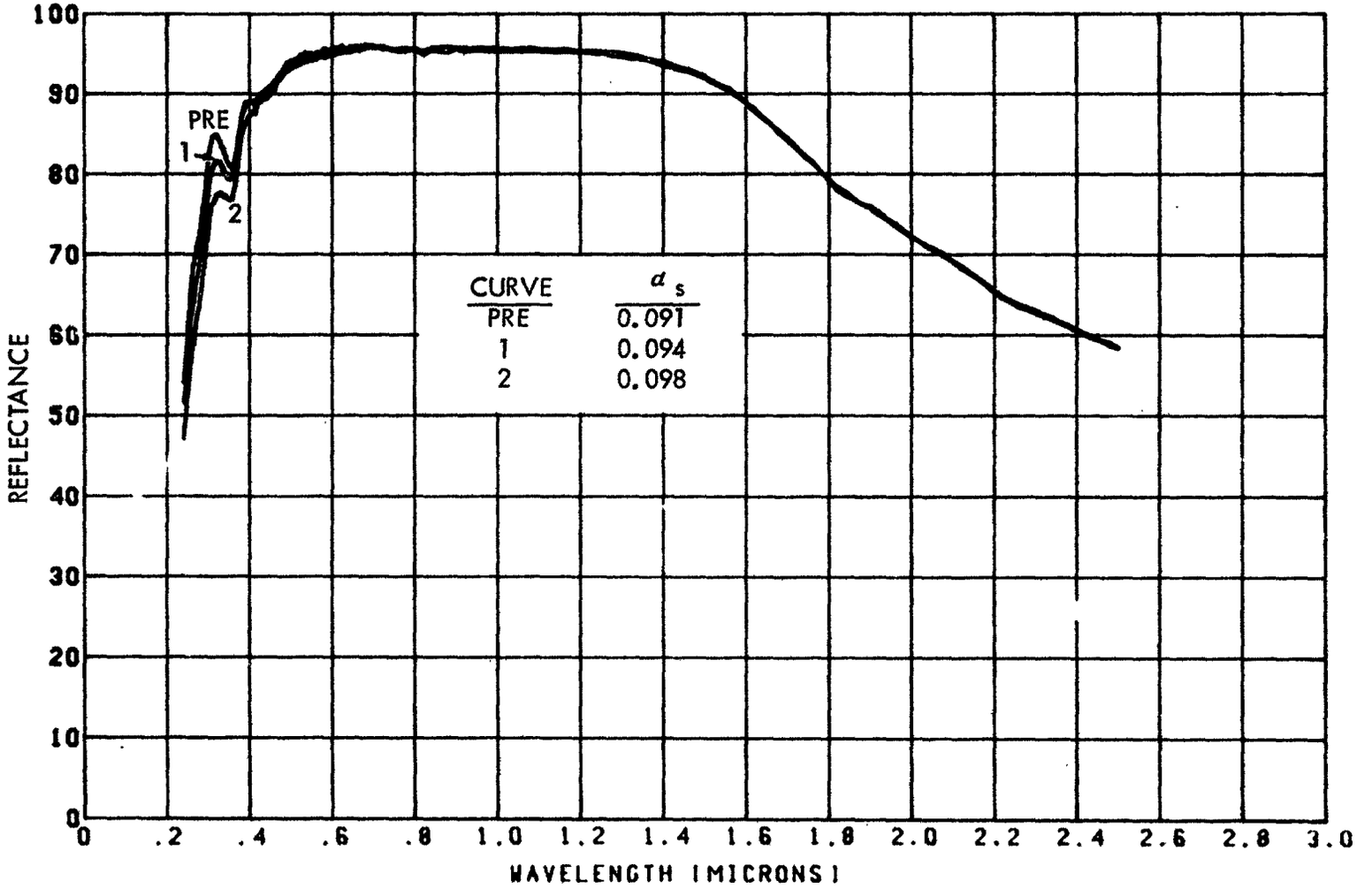

FIGURE A-7.

IN SITU EFFECTS OF 1-KEV PROTONS AND THERMAL ELECTRONS ON NASA-AMES AL_2O_3 ALPHA ALUMINUM OXIDE PIGMENT IN POTASSIUM SILICATE 1

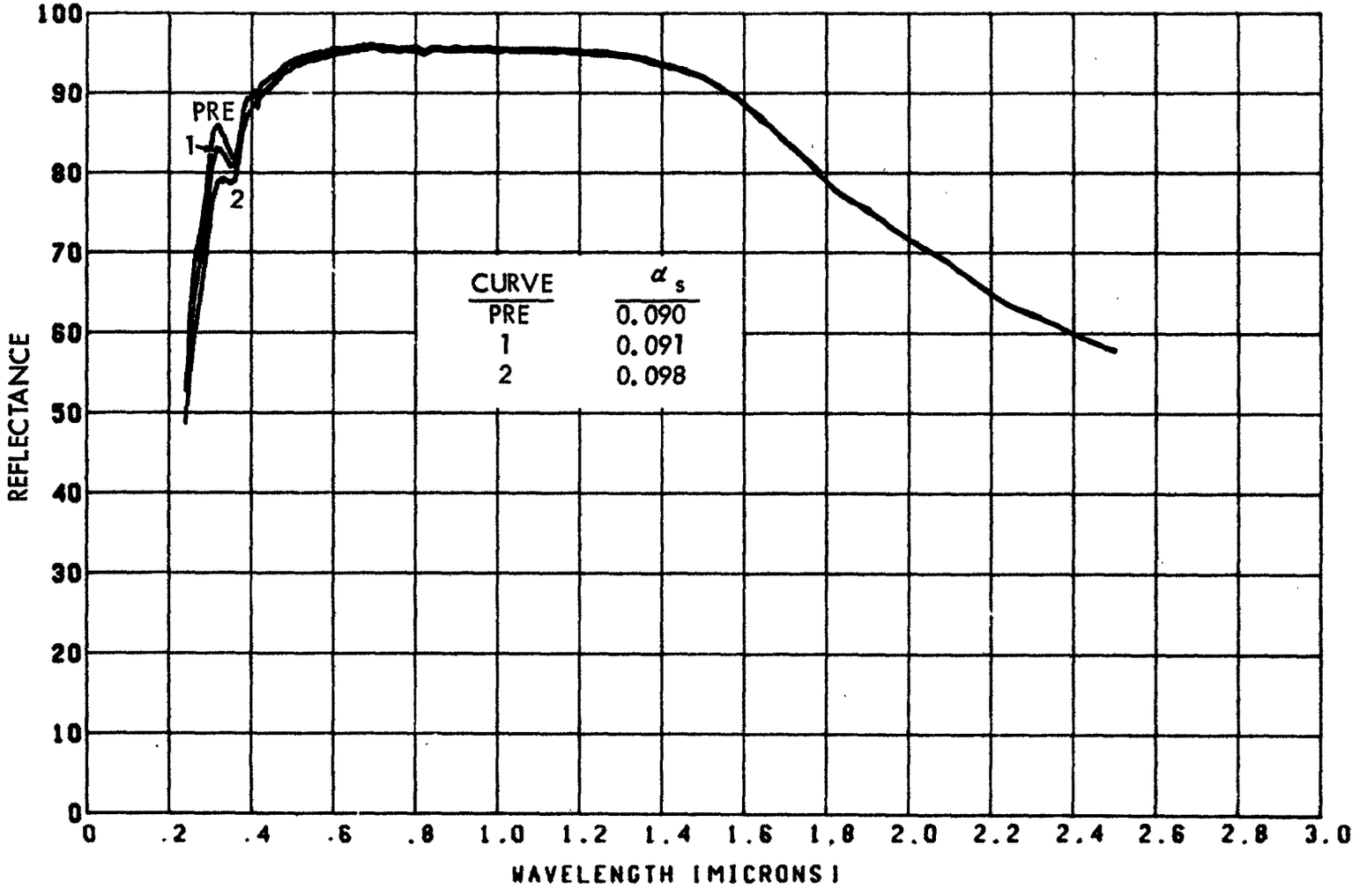

FIGURE A-8.

IN SITU EFFECTS OF THERMAL ELECTRONS AND ULTRAVIOLET ON NASA-AMES AL_2O_3 ALPHA ALUMINUM OXIDE PIGMENT IN POTASSIUM SILICATE 51

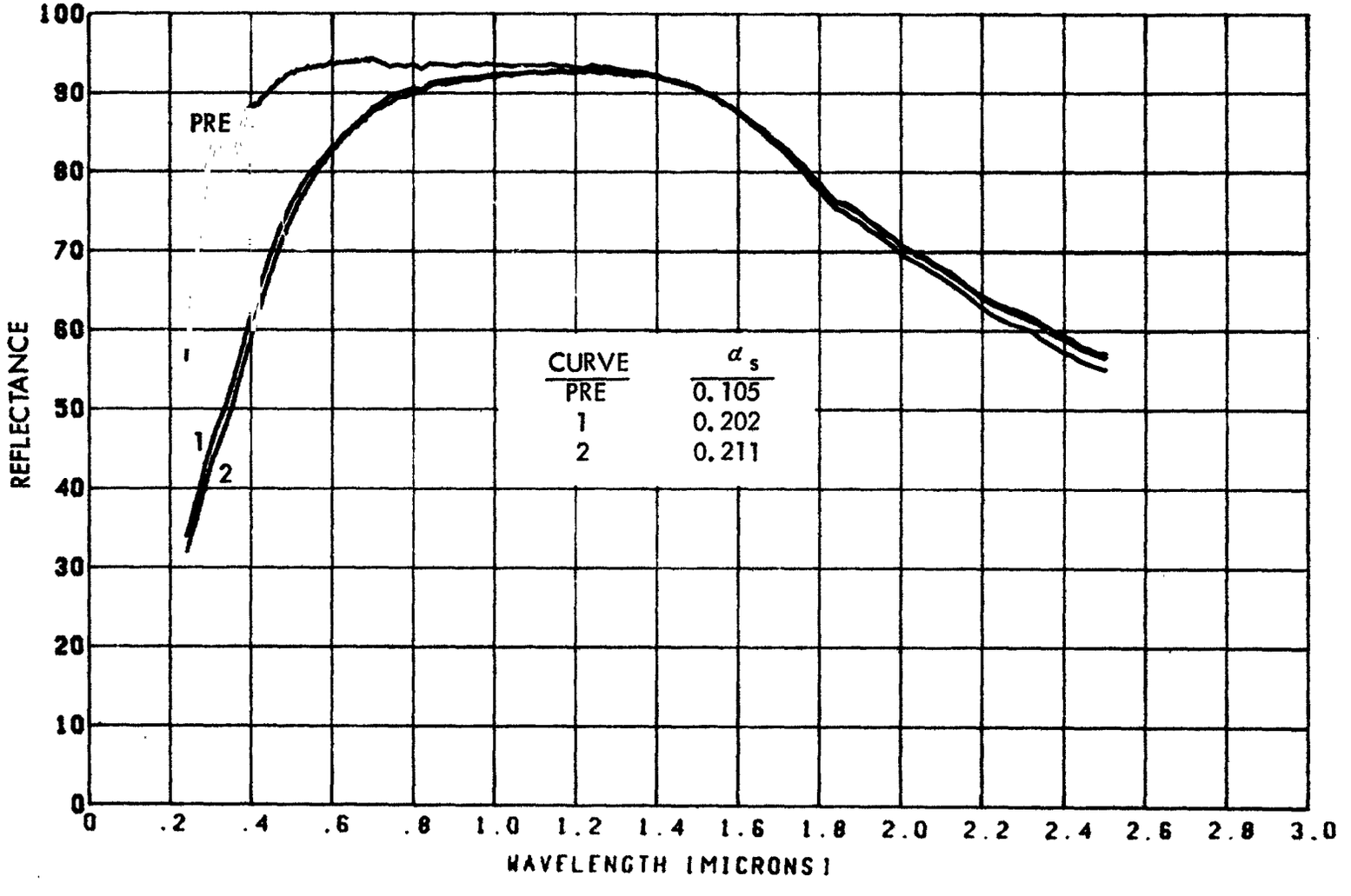

FIGURE A-9.

IN SITU EFFECTS OF 1-KEV PROTONS AND ULTRAVIOLET RADIATION ON NASA-AMES AL_2O_3 ALPHA ALUMINUM OXIDE PIGMENT IN POTASSIUM SILICATE 12

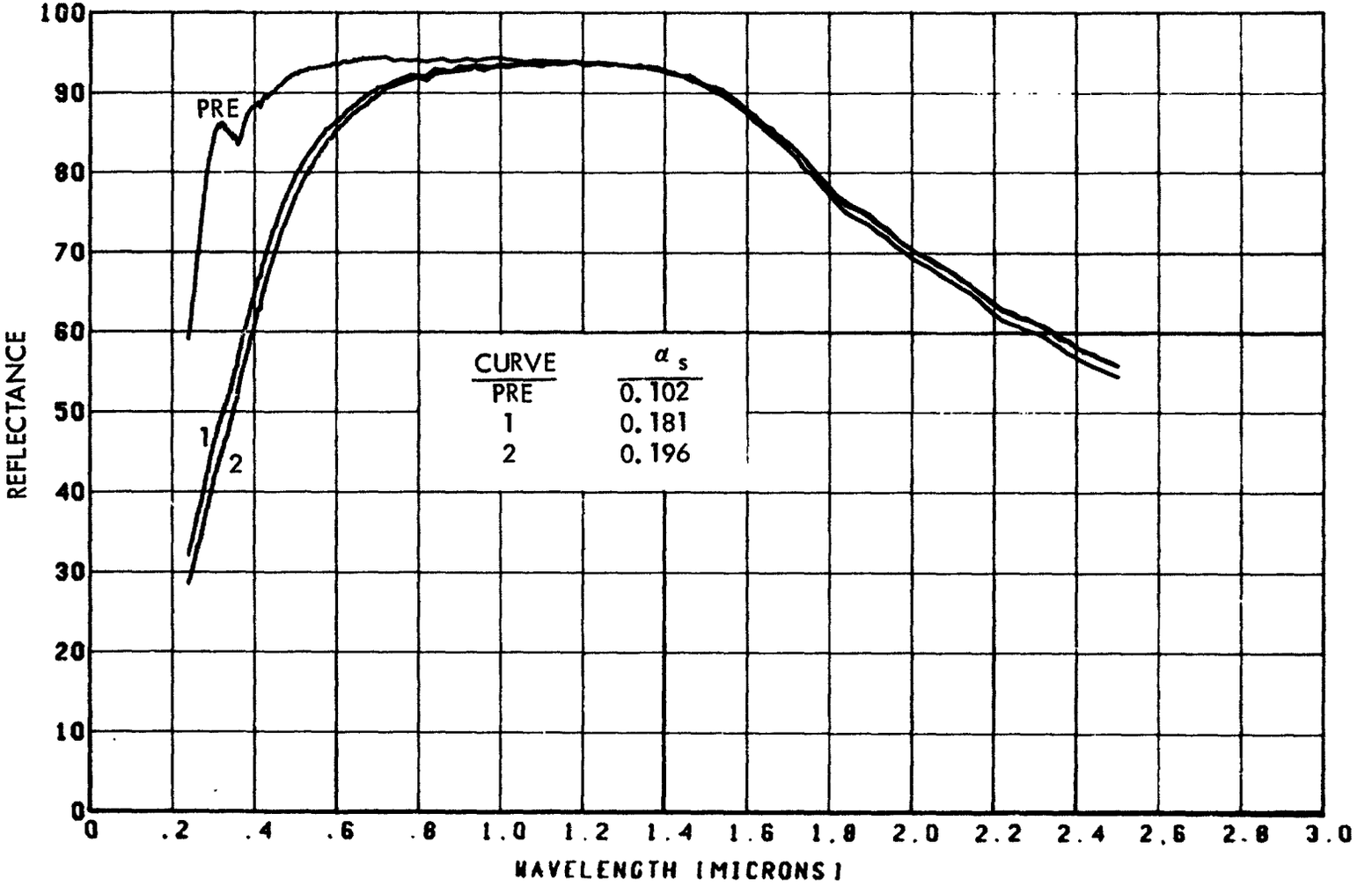

FIGURE A-10.

IN SITU EFFECTS OF 1-KEV PROTONS, THERMAL ELECTRONS, AND UV ON NASA-AMES AL_2O_3 ALPHA ALUMINUM OXIDE PIGMENT IN POTASSIUM SILICATE 4

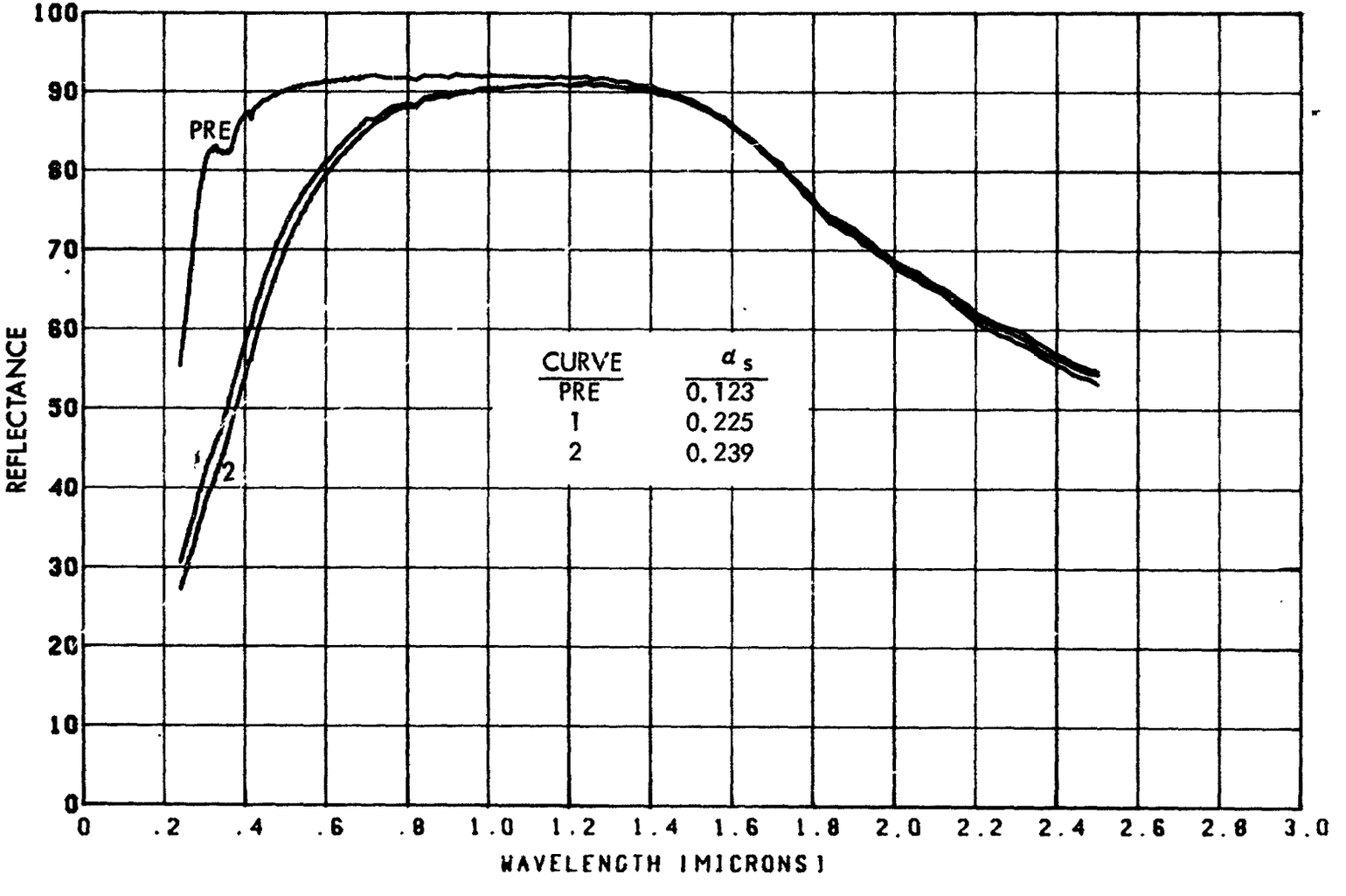

FIGURE A-11.

REFLECTANCE RECOVERY IN AIR AFTER UV EXPOSURE OF NASA-AMES Z-93 SP-500 ZINC OXIDE PIGMENT IN POTASSIUM SILICATE 45

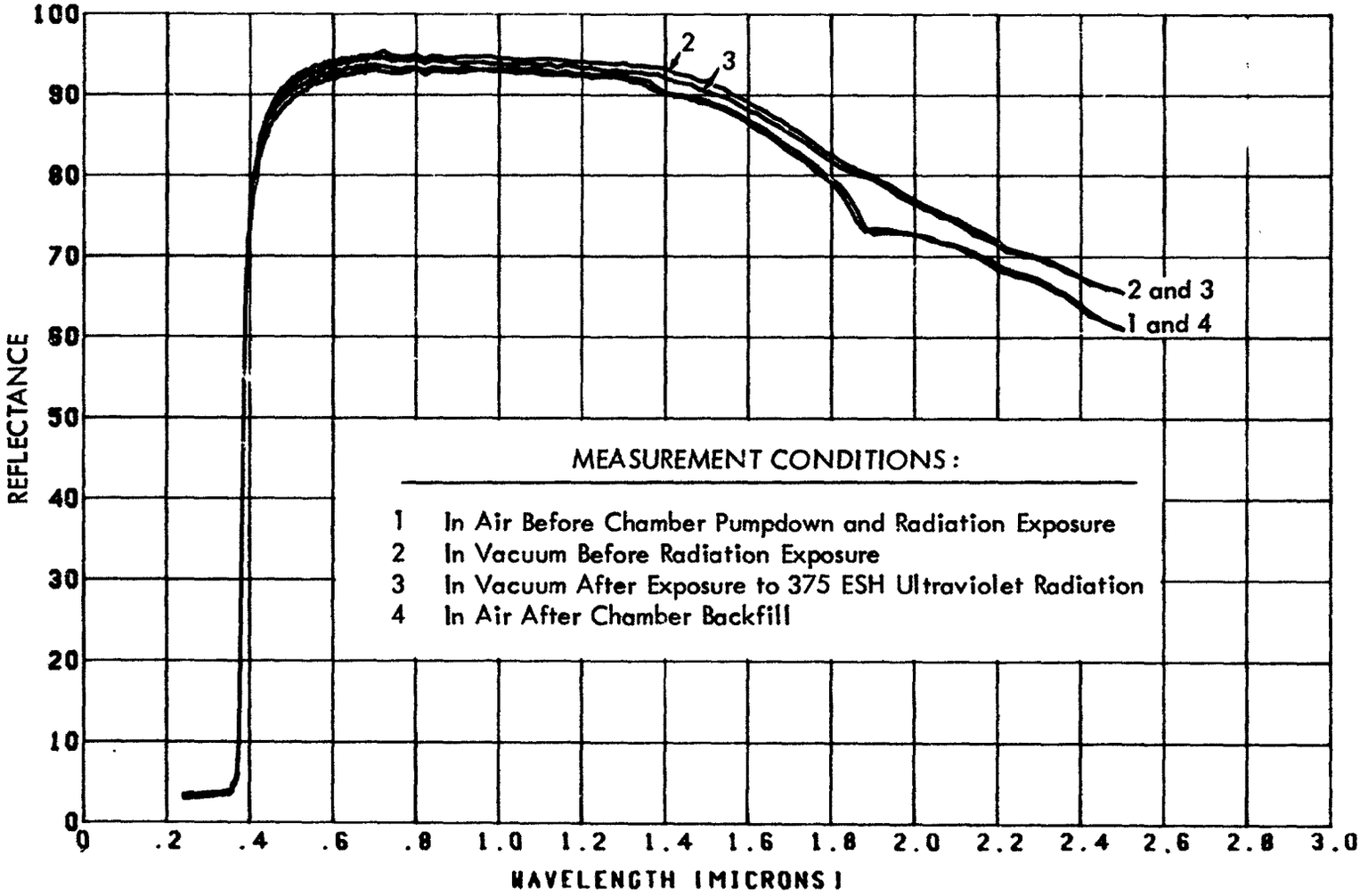

FIGURE A-12.

REFLECTANCE RECOVERY IN AIR AFTER UV EXPOSURE OF NASA-AMES AL203 ALPHA ALUMINUM OXIDE PIGMENT IN POTASSIUM SILICATE 70

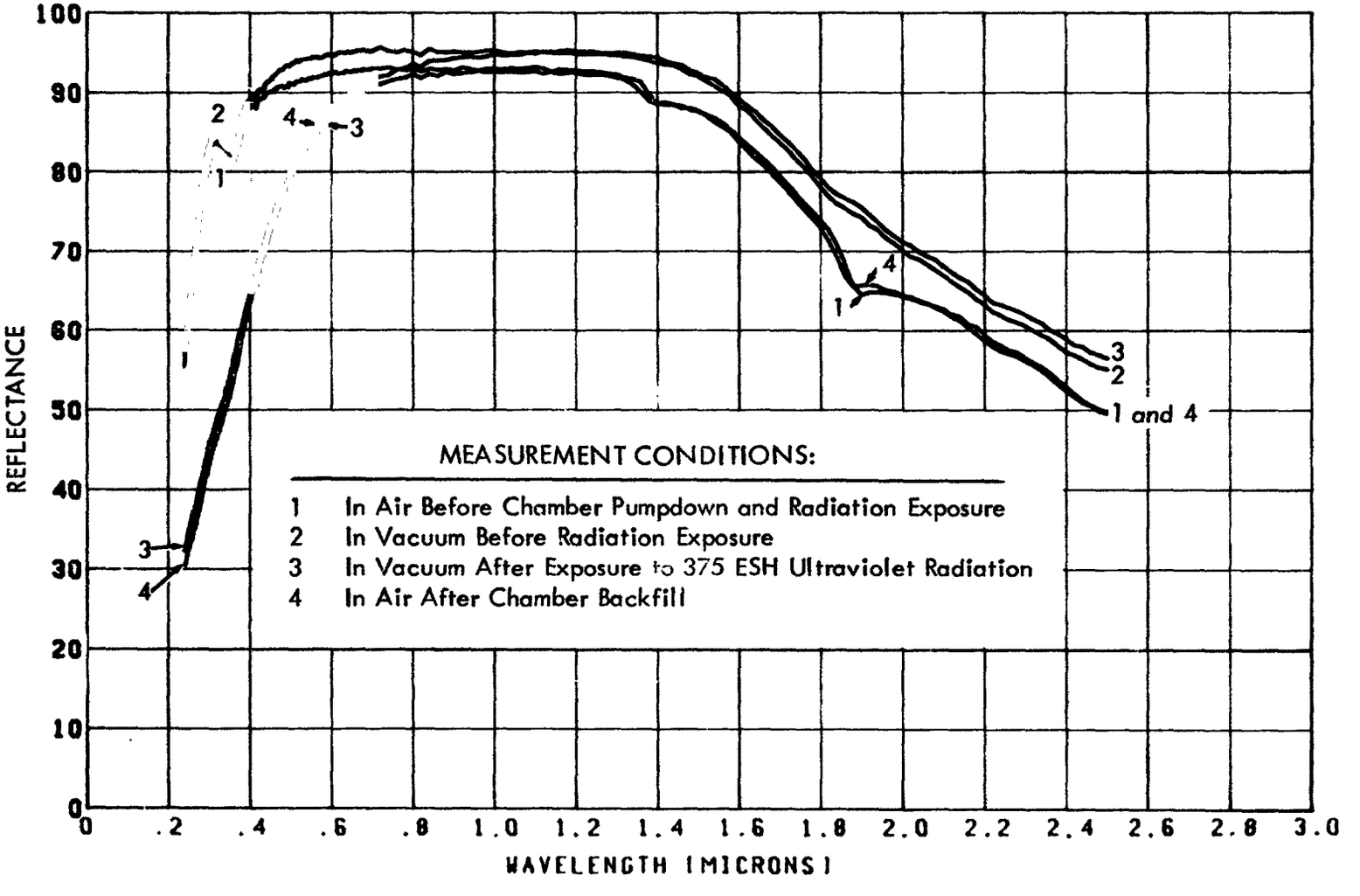

APPENDIX B

RELATIONSHIP OF PRESENT PROGRAM TO EARLIER NEUTRAL-BEAM WORK

Initial efforts were made at Boeing in 1968 to expose representative white-pigmented thermal control coatings to neutralized solar proton radiation. These first tests utilized 20-keV protons in simultaneous exposures with ultraviolet radiation at a rate of approximately one space sun. As in the present program, duplicate exposures except for the presence or absence of 45-eV "thermal" electrons were conducted. Reflectance-changing effects were studied in S-13G (silicate-treated zinc oxide pigment in methyl silicone binder) and in Pyromark (titanium dioxide pigment in methyl phenyl silicone binder). In S-13G, which is rather ultraviolet-stable but proton-degradable, severe reflectance degradation occurred in a wavelength band in the visible region (Figure B-1). Neutralization of the proton beam with thermal electrons resulted in only slightly greater damage, both in the visible and in the infrared wavelength region, where much smaller ΔR effects were measured. In Pyromark, which is quite susceptible to ultraviolet radiation-induced damage as well, reflectance degradation took place throughout the wavelength region from 0.4 to beyond 2.0 microns. Somewhat greater reflectance damage occurred as a result of exposure to thermal electrons along with protons and ultraviolet radiation (Figure B-2).

After these results were obtained, Farnsworth and others conducted an exploratory study of the effects of thermal electrons on the same coatings employed in the present program. This study reported substantially less spectral reflectance degradation occurring in coating samples exposed to thermal electrons simultaneously with either (a) 1-keV protons or (b) proton/ultraviolet radiation, compared with degradation occurring in proton or proton/ultraviolet exposures (respectively) without thermal electrons (Reference 9). Also reported was considerably less spectral and α_s damage in Al_2O_3—K_2SiO_3 after simultaneous particle/ultraviolet exposures than after ultraviolet-only exposure. There are several potential reasons for these

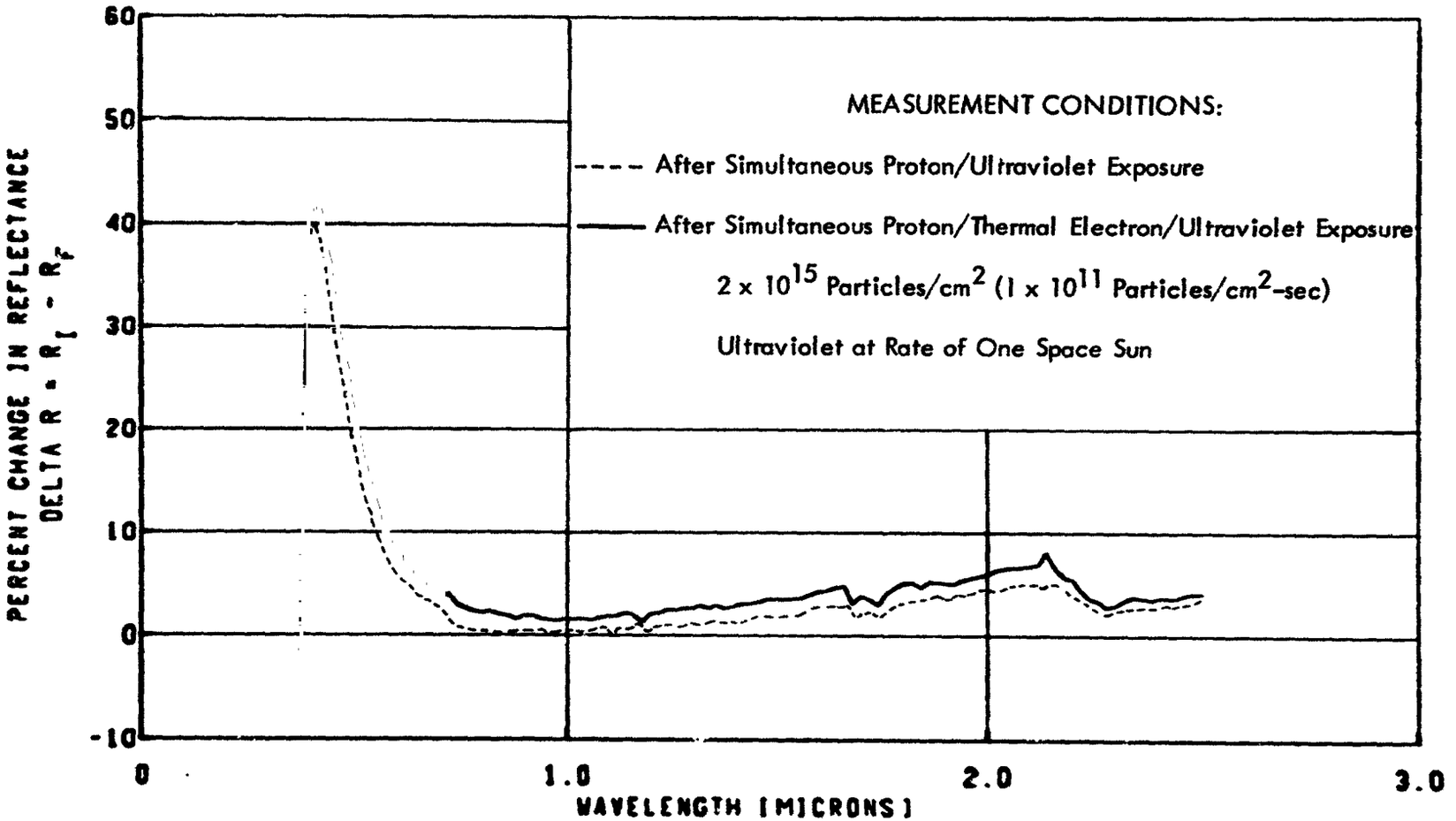

Figure B-1. In Situ Effects of Proton Beam Neutralization With Thermal Electrons on the Reflectance of S-13G

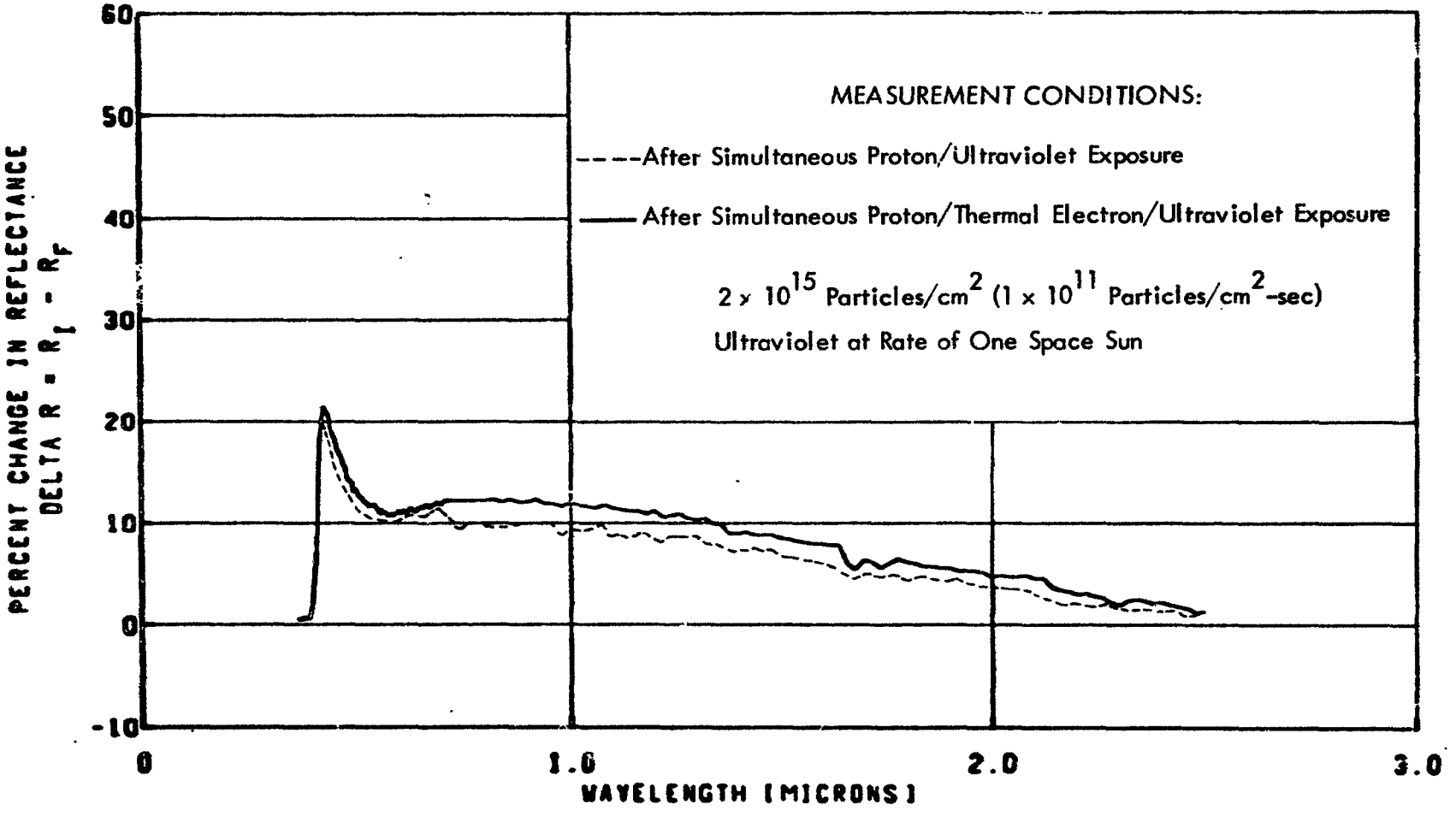

Figure B-2. In Situ Effects of Proton Beam Neutralization With Thermal Electrons on the Reflectance of Pyromark

observations in contrast with those of the present program. The isolation of protons from their mixed ion source output was somewhat in doubt, due to no magnetic analysis, proximity of ion source to samples, and poor vacuum levels during exposure. Various samples received considerably different particle exposure fluences due to nonuniform particle flux across the exposure beam. Total ideal exposure was to be 2×10^{15} particles/cm^2 with 375 ESH ultraviolet radiation simultaneously on appropriate samples. Thus a different ratio of particle/ultraviolet exposure was involved. Finally, whereas in the present program particle-only exposures have been perfomed separately in the dark, particle-only results from this earlier study were based on exposure with an attendant background of light reflected onto "particle-only" samples from various portions of the environmental chamber. In view of indicated interactions between proton and photon radiation, these differences should be kept in mind if results and conclusions from the two programs are compared.

REFERENCES

1. Handhausen, Barne, and Ness, J. Geophys. Res. 72, 5265 (1967).

2. Neugebauer and Snyder, "Average Properties of the Solar Wind as Determined by Mariner II," NASA N67-10253 (1966).

3. Lazarus, Bridge, and Davis, "Preliminary Results from the Pioneer 6 MIT Plasma Experiment," J. Geophys. Res. 71, 3790 (1966).

4. Barne, Handhausen, Asbridge, and Strong, Trans, Am. Geophys. Union 49, 262 (1968).

5. L. A. Frank, Trans. Am. Geophys. Union 49, 262 (1968).

6. R. R. Brown, L. B. Fogdall, and S. S. Cannaday, "Electron-Ultraviolet Radiation Effects on Thermal Control Coatings." Progress in Astronautics and Aeronautics, Volume 21, 1969.

7. L. B. Fogdall, S. S. Cannaday, and R. R. Brown, "In Situ Effects of Protons and Solar Electromagnetic Energy on Thermal Control Coatings," Proc. of 3rd Annual Space Symposium, (I. E. S.) Seattle, Sept. 1968.

8. L. B. Fogdall and S. S. Cannaday, "In Situ Electron, Proton, and Ultraviolet Radiation Effects on Thermal Control Coatings." Final Report for NASA-Goddard Contract NAS5-9650; Boeing Document D2-84118-9. January, 1969.

9. D. Farnsworth, "Exploratory Experimental Study on Neutral Charge Low Energy Particle Irradiation of Selected Thermal Control Coatings." Report for NASA-Ames Contract NAS2-4962, CR 73290, January, 1969.

10. L. B. Fogdall and S. S. Cannaday, "Dependence of Thermal Control Coating Degradation Upon Electron Energy." Final Report for NASA-Goddard Contract NAS5-11164, Boeing Document D2-126114-1, May, 1969

11. R. B. Gillette, R. R. Brown, R. F. Seiler, and W. R. Sheldon, "Effects of Protons and Alpha Particles on Thermal Properties of Spacecraft and Solar Concentrator Coatings." Progress in Astronautics and Aeronautics, Vol. 18, ed. G. B. Heller, pp. 413-440, New York Academic Press, 1966

BIBLIOGRAPHY

"Study of Color Center Formation in White Powder Compounds," by H. Levin, V. R. Honnold, and C. C. Berggren. NASA Report CR 73337 for Contract NAS2-5034, July, 1969